HHS Public Access

Author manuscript

Nat Plants. Author manuscript; available in PMC 2021 July 25.

Published in final edited form as:

Nat Plants. 2021 February ; 7(2): 184–197. doi:10.1038/s41477-020-00843-4.

UVR8 interacts with *de novo* DNA methyltransferase and suppresses DNA methylation in *Arabidopsis*

Jianjun Jiang[1,2], **Jie Liu**[2], **Dean Sanders**[2], **Shuiming Qian**[2], **Wendan Ren**[3], **Jikui Song**[3], **Fengquan Liu**[1,*], **Xuehua Zhong**[2,4,*]

[1]Institute of Plant Protection, Jiangsu Academy of Agricultural Sciences, Jiangsu Key Laboratory for Food Quality and Safety-State Key Laboratory Cultivation Base of Ministry of Science and Technology, Nanjing, Jiangsu 210014, China

[2]Laboratory of Genetics & Wisconsin Institute for Discovery, University of Wisconsin-Madison, Madison, WI 53706, USA

[3]Department of Biochemistry, University of California, Riverside, California 92521, USA

[4]Lead Contact

Abstract

DNA methylation is an important epigenetic gene regulatory mechanism conserved in eukaryotes. Emerging evidence shows DNA methylation alterations in response to environmental cues. However, the mechanism of how cells sense these signals and reprogram the methylation landscape is poorly understood. Here, we uncovered a novel connection between ultraviolet B (UVB) signaling and DNA methylation involving UVB photoreceptor (UVR8) and a *de novo* DNA methyltransferase (DRM2) in *Arabidopsis*. We demonstrated that UVB acts through UVR8 to inhibit DRM2-mediated DNA methylation and transcriptional de-repression. Interestingly, DNA transposons with high DNA methylation are more sensitive to UVB irradiation. Mechanistically, UVR8 interacts with and negatively regulates DRM2 by preventing its chromatin association and inhibiting the methyltransferase activity. Collectively, this study identifies UVB as a potent

*Correspondence: fqliu20011@sina.com (F.L.), xuehua.zhong@wisc.edu (X.Z.).

Author contributions

JJ designed and performed most experiments, analyzed data, prepared figures, and wrote the manuscript draft. JL and DS performed the genomic data analysis. SQ provided reagents and edited the manuscript. WR and JS provided recombinant DRM2 proteins. FL conceived the project and edited the manuscript. XZ conceived the project, designed experiments, analyzed data, and wrote the manuscript.

Supplementary information

Supplementary information can be found online.

Supplementary information

Supplementary Figures and Tables

Supplementary Figures 1–6 and Supplementary Tables 1–3.

Supplementary Datasets

Supplementary Dataset 1: List of proteins identified in IP-MS

Supplementary Dataset 2: UVB induced CHH DMRs

Supplementary Dataset 3: List of differentially expressed genes in UVB treated plants and in *dd* mutant

Competing interests

The authors declare no competing interests.

inhibitor of DNA methylation and provides mechanistic insights into how signaling transduction cascades intertwine with chromatin to guide genome functions.

DNA methylation is a conserved mechanism for gene regulation and plays quintessential roles in transposon silencing, imprinting, development, and environmental responses[1,2]. The predominant form of DNA methylation in eukaryotes occurs on 5-methylcytosine ($5^{m}C$), although adenine methylation has also been reported[3]. In plants, methylation is present in transposons, repetitive sequences, and gene bodies in three sequence contexts: CG, CHG, and CHH (H = A, T, or C)[4,5]. In *Arabidopsis*, the maintenance of DNA methylation is mediated by distinct pathways. CG and CHG methylation are maintained by METHYLTRANSFERASE 1 (MET1) and CHROMOMETHYLASE 3 (CMT3), respectively, while CHH methylation is maintained by DOMAINS REARRANGED METHYLTRANSFERASE 2 (DRM2) through the RNA-directed DNA methylation (RdDM) pathway and CHROMOMETHYLASE 2 (CMT2)[6,7]. While DRM2 is responsible for CHH methylation of euchromatic regions, short transposable elements (TEs), and the edges of long TEs, CMT2 preferentially methylates pericentromeric heterochromatin and the bodies of long TEs[8,9]. DNA methylation in all sequence contexts is established by the *de novo* activity of DRM2 through RdDM pathway[6,10,11].

Accumulating evidence suggests a functional link between DNA methylation and various developmental and environmental cues in both plants and mammals. Distinct DNA methylation patterns are established in different cell types and tissues and are tightly modulated during growth and development[12,13]. For example, maternal nutritional status during early pregnancy causes persistent and systemic epigenetic changes as metastable epialleles in humans[14]. In plants, distinct DNA methylation patterns have been reported in different cell types and tissues. For example, the genome of columella root cap cells is the most highly methylated in *Arabidopsis*, whereas soybean root hairs are more hypermethylated than stripped roots[15,16]. DNA methylation is also dynamically regulated by versatile environmental stimuli including herbicide, bacterial pathogen infection, salicylic acid treatment, ultraviolet radiation, heat stress, and microgravity during spaceflight[16–21]. In *Arabidopsis*, bacterial (*Pseudomonas syringae*) infection induces both hyper- and hypo-methylation at numerous regions, among which many are correlated with gene expression changes[18]. The *Arabidopsis* plants grown in the international space station have higher methylation levels in the context of CHG and CHH within protein-coding genes compared with those of ground grown plants[21]. Despite the large amount of the descriptive information regarding the dynamic DNA methylation patterns in response to environmental cues, the underlying mechanism is poorly understood.

Ultraviolet-B (UVB) is an inherent part of sunlight that can penetrate the atmosphere of earth and affect many biological processes[22]. In plants, natural low-level and non-damaging UVB acts as a signal to regulate development and assimilation, such as inhibition of hypocotyl elongation and biosynthesis of flavonoids and anthocyanins for UVB protection[23]. In *Arabidopsis*, UV RESISTANCE LOCUS 8 (UVR8) is the photoreceptor of UVB[24]. UVR8 predominately exists in the cytosol as an inactive homodimer, and upon UVB exposure, it undergoes monomerization due to the disruption of π-cation interactions

after absorption of UVB by tryptophan chromophores and is imported into the nucleus[24–26]. In the absence of UVB, UVR8 monomers re-dimerize with the assistance of REPRESSOR OF UVB PHOTOMORPHOGENESIS (RUPs), a class of WD40-repeat proteins[27]. Downstream of UVB perception, UVR8 interacts with E3 ligase CONSTITUTIVELY PHOTOMORPHOGENIC 1 (COP1), transcription factors WRKY DNA BINDING PROTEIN 36/13 (WRKY36/13), MYB DOMAIN PROTEIN 73/77 (MYB73/77), BRI1-EMS-SUPPRESSOR 1 (BES1), and BES1-INTERACTING MYC-LIKE 1 (BIM1) to transduce UVB signals[24,28–31]. Previous studies suggest a potential role of DNA methylation in adaptation to high UVB irradiation for high-altitude maize landraces[32]. High-altitude related human disorders (e.g. pulmonary edema) are also associated with aberrant DNA methylation[33]. Despite the correlative information, how distinct DNA methylation patterns are established and maintained in response to UVB exposure remains unknown.

In this study, we found that UVB acts through DRM2 to suppress DNA methylation and de-repress several reporter genes in a UVR8 dependent manner. Genome-wide DNA methylation analysis further showed that UVB induced DNA hypomethylation preferentially around pericentromeric regions and TEs. The UVB photoreceptor UVR8 directly interacts with DNA methyltransferase DRM2 in the nucleus and that this interaction is mediated by the ubiquitin-associated (UBA) domains of DRM2. Mechanistic dissection of UVR8 action on DRM2 revealed that UVR8 does not impact DRM2 protein stability and nuclear accumulation. Instead, UVR8 inhibits DRM2 chromatin association and catalytic activity. Collectively, this study identifies UVR8 as a negative regulator of DRM2 and establishes a mechanistic connection between light signaling and DNA methylation in plants.

Results

UVB induces DNA hypomethylation and de-represses reporter genes

Our prior immunoprecipitation coupled with mass spectrometry (IP-MS) experiments of DNA methyltransferase DRM2 identified ARGONAUTE 4 (AGO4)[34] and the ultraviolet B (UVB) photoreceptor, UVR8, which perceives UVB and induces physiological responses to secure plant acclimation and thus promotes survival in sunlight[23] (Supplementary Dataset 1). This leads us to hypothesize that UVB may be connected to DNA methylation. To determine whether UVB has an impact on DNA methylation, we first utilized a dual Cauliflower Mosaic Virus *35S* promoter driven luciferase (*d35S:LUC*) reporter system (Fig. 1a), where *d35S* promoter regions are methylated and the *LUC* gene is transcriptionally inhibited[35]. A novel medium *d35S:LUC* line (*LUCM*) was used as it is methylated at a medium level and thus could reveal the change of DNA methylation in both directions (Extended Data Fig. 1a–e). When crossing *LUCM* into *drm1 drm2* (*dd*) background, LUC intensity was increased and DNA methylation at *d35S* promoter was reduced (Extended Data Fig. 1f,g). Upon UVB irradiation, we noted an increased LUC intensity in *LUCM* compared to the plants grown under white light (Fig. 1b,c). Further examination of the DNA methylation at the *35S* promoter by McrBC (a nuclease cleaves DNA containing ^{m}C) digestion and bisulfite sequencing revealed decreased DNA methylation levels in response to UVB treatment (Fig. 1d,e). Next, we asked whether UVB-induced DNA hypomethylation is mediated by DRM2. We utilized another reporter line where GFP expression is driven by the

promoter of the *SDC* (*SUPPRESSOR OF DRM2 CMT3*) gene. The *SDC* gene has 7 tandem repeats in its promoter region and is silent in wild-type plants and only becomes demethylated and transcriptionally reactivated when both DRM2 and CMT3 pathways are inactivated[36]. When introducing *pSDC:GFP* into the *cmt3* null mutant[36], we noted an increased GFP protein abundancy accompanied by a significant increase in the endogenous *SDC* transcript levels with UVB treatment (Fig. 1f,g), suggesting that UVB acts through DRM2 to alter DNA methylation.

UVR8 mediates UVB-induced DNA hypomethylation

As UVR8 is the photoreceptor of UVB, we asked whether UVB induced DNA methylation depends on UVR8. We crossed the *LUCM* with *uvr8–6* and also *cop1–6*, in which the UVR8 signaling downstream component COP1 is mutated[37]. Under white light, we found that luciferase luminescence and *LUC* RNA transcript levels in *uvr8–6 LUCM* were both reduced compared with *LUCM*, while *cop1–6 LUCM* was similar to *LUCM* (Fig. 1h,i). We next assessed DNA methylation levels in these lines by McrBC digestion and found that the DNA methylation of *d35S* promoter regions was significantly increased in *uvr8–6 LUCM* compared to *LUCM* (Fig. 1j), suggesting that UVR8 induces DNA hypomethylation. We next investigated the impact of UVB on *LUC* intensity and found that unlike *LUCM* and *cop1–6 LUCM* plants, the *LUC* intensity in *uvr8–6* is similar in white light and UVB treatment (Fig. 1k), suggesting that *LUC* is insensitive to UVB when UVR8 is absent. It further suggests that UVR8 mediates UVB-induced DNA methylation reduction.

We next investigated whether UVR8 overexpression can lead to DNA methylation alteration. We transformed *FLOWERING WAGENINGEN* (*FWA*) transgene, which is not methylated and can be *de novo* methylated by the DRM2 pathway[38], into *35S*:*UVR8-FLAG* overexpressing lines (*UVR8-OX*, Supplementary Fig. 1). When grown under white light generated by fluorescent tubes producing a low level of UVB[39], *FWA*/*UVR8-OX* plants showed a significant late flowering phenotype compared with *FWA*/Col-0 in both T_3 homozygous and T_1 transgenic populations (Fig. 1l,m and Extended Data Fig. 2). Furthermore, *FWA* transgene in lines expressing a constitutively monomeric $UVR8^{W285A}$ showed even later flowering compared with *FWA*/*UVR8-OX* (Extended Data Fig. 2b). These data indicate that *UVR8* overexpression inhibited the *de novo* methylation of *FWA* transgene. To determine whether UVR8 acts through DRM2 to regulate *FWA* methylation, we generated *uvr8–6 drm1 drm2* (*udd*) triple mutant. *FWA*/*udd* transgenic plants demonstrated late flowering to a similar extent of *FWA*/*dd* (Extended Data Fig. 2a). Further examination of another locus (*Chr1:23068006*) methylated by DRM2 revealed increased DNA methylation in all CG, CHG, and CHH contexts in *uvr8–6*, which was abolished in the triple *udd* mutant (Fig. 1n). Together, these data suggest that UVR8 mediates UVB-induced DNA hypomethylation.

UVB induces genome-wide DNA hypomethylation

To further investigate the impact of UVB on the DNA methylation, we examined two endogenous loci: *Chr1:23068006* and *AtSN1,* a well-characterized retrotransposon whose methylation is dependent on DRM2[40]. Upon UVB treatment, we noted a slight reduction of DNA methylation in Col-0 and the reduction was further enhanced in *UVR8-OX* plants (Fig.

2a), indicating that UVB reduces DNA methylation in a UVR8-dependent manner. To determine whether UVB alters global DNA methylation, we performed whole-genome bisulfite sequencing (Supplementary Table 1) and found no notable global methylation difference between Col-0 plants grown under white light (WL) or UVB. In contrast, the UVB treated *UVR8-OX* showed a great reduction of CHH methylation particularly at the centromeric and pericentromeric regions (Fig. 2b). Consistently, we found that UVB-induced differentially methylated regions (DMRs) in both Col-0 and *UVR8-OX* are mostly in the context of CHH with majority of hypo DMRs (Fig. 2c). We next compared UVB-induced CHH hypo DMRs with that of the *drm1 drm2* (*dd*), *drm2–2*, and *cmt2–3*. We found that ~55% and ~61% of UVB induced DMRs in Col-0 overlap with *dd* DMRs and *drm2–2* DMRs, respectively (Fig. 2d, Extended Data Fig. 3a–c and Supplementary Dataset 2). Besides DRM2, we also found that 635 out of 5189 (~12%) UVB-induced CHH hypo DMRs are uniquely overlapped with *cmt2*-DMRs (Extended Data Fig. 3a). Significant CHH methylation reduction was observed in UVB-treated Col-0 and more drastically in *UVR8-OX* at both UVB-specific and overlapping DMRs with *dd*-DMRs (Fig. 2d,e and Extended Data Fig. 3b,c). Interestingly, *dd*-specific DMRs also showed a significant decrease of CHH methylation by UVB treatment comparing with non-treated control in both Col-0 and *UVR8-OX* (Fig. 2d,e), suggesting that these regions are likely weak UVB targets despite being called as not significant DMRs. We further noticed that UVR8 overexpression alone without UVB treatment also showed a relatively mild CHH methylation reduction, both globally and at specific loci (Fig. 2d–f). In addition, we performed bisulfite sequencing of *uvr8–6* mutant with or without UVB treatment (Supplementary Dataset 2) and found very little DNA methylation changes at genome wide level comparing *uvr8–6* with Col-0 under white light (Extended Data Fig. 3d). We also noticed that only a very small fraction of UVB-induced CHH hypo DMRs in *uvr8–6* overlap with those in Col-0, suggesting that the UVB induced DMRs mostly depend on UVR8 (Extended Data Fig. 3e).

We next profiled the genome distribution pattern of UVB-induced CHH hypo DMRs and found that UVB-DMRs are enriched in promoters and TEs, similar to those of *dd*-DMRs (Fig. 2g). These UVB-induced DMRs were co-localized with TEs, especially in pericentromeric regions (Fig. 2h). TEs containing UVB-induced DMRs tend to have much higher CHH methylation level than that of TEs without UVB- DMRs (Fig. 2i), indicating that the TEs with high CHH methylation were more sensitive to UVB. Moreover, long TEs (>500 bp) and certain types of Class II DNA transposons were enriched with UVB-induced DMRs, similar to the pattern of TEs containing *dd*-DMRs (Extended Data Fig. 3f,g). Further comparison of UVB-induced DMRs with published UVC-induced DMRs (ref[41]) revealed a very small portion of overlapping DMRs (Extended Data Fig. 4a–d), suggesting that the UVB-induced DMRs identified in this study were not induced by DNA damaging. In summary, these data demonstrate that UVB induces genome-wide DNA methylation reduction with preference over TEs with high CHH methylation and long Class II DNA transposons.

UVB and DRM2 de-repress a set of TEs

To determine the transcriptional changes induced by UVB, we first checked the transcription of *Romania T5* and *AtCopia28*, two TEs repressed by DNA methylation, and found that they

were significantly upregulated in UVB treated *pSDC:GFP/cmt3* plants (Fig. 3a). We next performed RNA-seq on Col-0 and *dd* with or without UVB treatment (Fig. 3b, Extended Data Fig. 5a, and Supplementary Table 2). The transcriptional responses to UVB are similar in Col-0 and *dd* with a large portion of overlapped differentially expressed genes (DEGs) and correlated fold-change of expression levels (Extended Data Fig. 5a,b). UVB-induced marker genes including *CHS*, *ELIP1, ELIP2*, and *RUP2* were upregulated in the UVB treated plants, while high-dosage DNA-damaging UVB-induced genes were unchanged (Extended Data Fig. 5c–e). Comparison of our RNA-seq data of 10-day UVB treatment with that of short-term (6 hours) treatment revealed that short-term UVB-treatment has stronger effect on gene expression in terms of both number of DEGs and fold-change (Extended Data Fig. 5f–h). Overlapping of the DEGs of UVB treated Col-0 and *dd* revealed that only a few genes are commonly regulated by DRM2 and UVB, suggesting that genes are not major targets of UVB-induced DNA hypomethylation (Fig. 3b, Supplementary Dataset 3). This is consistent with the fact that DNA methylation primarily suppresses TE in *Arabidopsis*[42]. Hence, we analyzed TE expression in our RNA-seq data and noticed more up-regulated TEs (269) than down-regulated TEs (65) (Fig. 3c, Supplementary Dataset 3). 96 up-regulated TEs were significantly overlapped between *dd* mutant and UVB-treated Col-0 (Fig. 3d,e,f). This was further confirmed by RT-qPCR of 5 selected TEs showing up-regulation in UVB-treated Col-0 and *UVR8-OX*, but no response to UVB in *uvr8–6* mutant (Fig. 3g). We further found reduced CHH methylation level in UVB-treated *UVR8-OX* over the upregulated TEs (Extended Data Fig. 5i).

UVB photoreceptor UVR8 interacts with DRM2 *in vitro* and *in vivo*

Our prior DRM2 IP-MS experiment identified 6–7 unique UVR8 peptides (Supplementary Dataset 1 and Fig. 4a). UVR8 was also found to be specifically pulled down by DRM2, but not by other chromatin factors (Extended Data Fig. 6a). To verify our IP-MS data, we first extracted total proteins from transgenic *Arabidopsis* expressing N-terminal tagged 3xFLAG-9xMyc-DRM2 in *dd* mutant background (*3F9M-DRM2*)[34] and incubated them with recombinant full-length GST-UVR8, which contains both monomeric and dimeric UVR8 (Extended Data Fig. 6b). DRM2 was co-precipitated with GST-UVR8, but not GST alone (Fig. 4b). Next, we co-infiltrated Agrobacterium carrying both *35S* promoter driven *UVR8-HA (UVR8-HA*) and DRM2 genomic sequence fused with 3xFLAG at C-terminus (*DRM2-FLAG*) in *Nicotiana benthamiana* leaves and found that UVR8 co-immunoprecipitated with DRM2 (Extended Data Fig. 6c). Similar co-purification was detected when using transgenic *Arabidopsis* plants co-expressing UVR8-HA and 3F9M-DRM2 (Extended Data Fig. 6d). UVR8-DRM2 interaction was further confirmed to be in the nucleus by Co-IP using isolated nuclei from these transgenic *Arabidopsis* plants (Fig. 4c). We also performed a split luciferase complementation assay by fusing N- and C-terminal domain of luciferase (nLuc and cLuc, respectively) to the full-length UVR8 and DRM2 and co-expressed them in *N. benthamiana* leaves. The co-infiltration of UVR8-nLuc and cLuc-DRM2 as well as DRM2-nLuc and cLuc-UVR8 showed strong luminescence signals compared to the negative controls (Fig. 4d,e). To determine whether UVB has an impact on UVR8-DRM2 interaction, we performed Co-IP experiment using the nuclei isolated from *UVR8-HA*/*3F9M-DRM2* transgenic plants treated with or without UVB and found that UVB enhanced the UVR8-DRM2 interaction in the nucleus (Fig. 4f). We also

irradiated only the half of *N. benthamiana* leaf with UVB with the other half of the same leaf covered with aluminum foil (Fig. 4g). Compared to the untreated side (-UVB), the half leaf treated with UVB showed stronger luciferase luminous intensity (Fig. 4h,i). This increased signal is due to enhanced interaction between DRM2 and UVR8 but not their protein level change (Extended Data Fig. 6e). Together, these data suggest that UVR8 interacts with DRM2 *in vitro* and *in vivo*.

DRM2 interacts with UVR8 in the nucleus via its UBA domains

We further investigated the subcellular localization of DRM2-UVR8 interaction by performing Bimolecular Fluorescence Complementation (BIFC) assay. Full-length UVR8 was fused with an N-terminus of YFP (nYFP-UVR8) and DRM2 was fused with C-terminal fragment of YFP (DRM2-cYFP). We found that UVR8 interacts with DRM2 in the nucleus in a pattern similar to the DRM2-DRM2 interaction (Fig. 5a), consistent with the dimerization of DRM2[34]. UVR8 is known to exist as a homodimer predominantly in the cytosol in normal condition and undergoes monomerization upon UVB exposure. We next investigated which form of UVR8 could interact with DRM2 by utilizing $UVR8^{W285A}$ and $UVR8^{W285F}$ mutants, constitutive monomeric and dimeric form, respectively[24]. The results of both split luciferase and BIFC assays showed that both $UVR8^{W285A}$ and $UVR8^{W285F}$ can interact with DRM2 in the nucleus (Fig. 5b and Extended Data Fig. 6f,g). *Arabidopsis* DRM2 contains three tandem ubiquitin-associated (UBA) domains at the N-terminus and a rearranged catalytic domain at the C-terminus[43]. To examine which domain mediates the interaction with UVR8, we generated two truncated DRM2 mutants containing only the UBA domains ($DRM2^{UBA}$) or catalytic domain ($DRM2^{CAT}$). The BIFC assay showed that the $DRM2^{UBA}$, but not $DRM2^{CAT}$, was able to interact with UVR8, suggesting that UBA domains are necessary and sufficient to mediate the DRM2-UVR8 interaction (Fig. 5a). We also truncated UVR8 into the core domain (1–396) and the C-terminus, both of which are important for interaction with COP1[44], and noted that both truncations can interact with DRM2 (Extended Data Fig. 7a). Interestingly, we found that UVR8 and its mutant forms all interact with DRM2 in certain nuclear bodies (Fig. 5c and Extended Data Fig. 7b). Notably, the UVR8-DRM2 nuclear body is distinct from AB body (AGO4/NRPD1B-body)[45]that is adjacent to nucleolus and is also different from COP1 nuclear bodies (Extended Data Fig. 6h). Taken together, these results suggest that the UBA domains in DRM2 are necessary and sufficient for UVR8 interaction.

UVR8 inhibits the catalytic activity and chromatin association of DRM2

The direct UVR8-DRM2 interaction (Figs. 4 and 5) and inhibition of DRM2-mediated DNA methylation by UVR8 (Figs. 1 and 2) suggest that UVR8 might negatively regulates DRM2. To dissect the molecular mechanism, we first determined whether UVR8 regulates DRM2 protein stability. We found no noticeable difference in DRM2 protein level with and without UVB treatment (Fig. 6a). Similarly, plants without UVR8 exhibit similar DRM2 abundance as those with UVR8 (Fig. 6b). Next, we assessed whether UVR8 affects DRM2 nuclear localization. Co-expression of UVR8-GFP or $UVR8^{W285A}$-GFP with DRM2-mCherry did not change the nuclear localization of DRM2 (Supplementary Fig. 2a–c). We also generated *DRM2-GFP* transgenic *Arabidopsis* plants in both *dd* and *udd* mutants and showed that neither UVR8 nor UVB affects DRM2 nuclear localization (Fig. 6c and Supplementary Fig.

2d). There was also no significant difference in the transcription levels of DRM2, other RdDM components, and proteins in DNA demethylation pathway in response to UVB (Supplementary Fig. 3a–c). These results suggested that UVB and UVR8 do not regulate DRM2 transcription, protein stability, and subcellular localization.

To test the role of UVR8 in DRM2 catalytic activity, we performed *in vitro* methyltransferase assay using recombinant DRM2 protein containing both UBA and CAT domains (59–626 aa). We found that DRM2 activity was similarly inhibited by UVR8, $UVR8^{W285A}$, and $UVR8^{W285F}$ (Fig. 6d). Interestingly, the DRM2 catalytic domain ($DRM2^{CAT}$, 269–626 aa) was insensitive to UVR8 (Supplementary Fig. 4a,b), consistent with the observation that UVR8 interacts with DRM2 via the UBA domains (Fig. 5). To test whether UVR8 regulates DRM2 chromatin association, we performed ChIP-qPCR using the flowers of *DRM2-FLAG* in *dd* and *udd* with or without UVB treatment. DRM2 showed enrichment at several loci, including *Chr1:23068006* and two TEs (AT4TE29620 and AT1TE55145) with decreased DNA methylation in *dd* and UVB irradiated samples (Fig. 2a,f). Interestingly, we noted significantly reduced DRM2 chromatin enrichment of these loci upon UVB irradiation (Fig. 6e). The DRM2 enrichment at these loci was not affected by UVB in *udd* when UVR8 is absent (Fig. 6e), suggesting that UVB inhibited DRM2 chromatin association is dependent on UVR8 at these loci.

Discussion

In this study, we have identified a novel mechanistic connection between ultraviolet light signaling and DNA methylation involving UVB photoreceptor UVR8 and a key *de novo* DNA methyltransferase DRM2. We showed that a direct physical interaction between UVR8 and DRM2 is critical for UVB-induced DNA methylation alternation and transcriptional de-repression. These findings suggest that UVR8 acts as a molecular sensor and transmits the UVB signaling to regulate DRM2-mediated DNA methylation. Here, we propose a working model wherein UVR8 predominantly localizes in the cytosol as a homodimer with a small portion in the nucleus to interact with DRM2 and exhibit a basal inhibitory activity on DRM2 under white light. Upon UVB exposure, UVR8 converts into an active monomer, which traffics into the nucleus and interacts with DRM2 to inhibit DRM2 activity, leading to DNA hypomethylation (Fig. 6f). The lower DNA methylation induced by UVB could be due to an inhibition of the maintenance process (passive demethylation) or an active DNA demethylation accompanied by an inefficient re-establishment of the methylation landscape. Whether UVB regulates active DNA demethylation needs to be further investigated, although UVB does not change the transcription of active DNA demethylation components (Supplementary Fig. 3b).

UVB has been reported to induce the dynamic DNA methylation change in different species. Consistent with our results in *Arabidopsis*, UVB exposure induces hypomethylation at several loci in maize, Norway spruce (*Picea abies*), and *Artemisia annua*[32,46–48]. Some studies showed no DNA methylation reduction by UVB[49] and even observed hypermethylation in grape[50]. Due to the limited number of tested loci in these species, it remains unclear whether UVB has distinct impact on global DNA methylation in different plant species. Similar UVB-induced dynamic DNA methylation patterns have been reported

in mammals, in which a UVB photoreceptor has yet to be discovered. In mice, DNA is hypermethylated in accompaniment with elevated expression of *DNMTs* in UVB-exposed epidermal skin and UVB-induced skin tumors[51]. In humans, UVB irradiation leads to decreased DNA methylation and *DNMT1* expression in T-cells of patients with systemic lupus erythematosus[52]. It should be noted that current knowledge of specific methylation patterns in these species is largely based on the genetic analyses of a few loci. The molecular mechanism(s) of establishing such dynamic DNA methylation patterns in response to UVB exposure in diverse plant and animal species is unknown. To our knowledge, the study presented here is the first mechanistic investigation of the impact of UVB on DNA methylation and provides a molecular mechanism linking UVB signaling pathway to DNA methylation.

Besides UVB, many other internal and external cues also alter the plant DNA methylome. Bacterial pathogen *P. syringae* pv. tomato DC3000 induces global hypomethylation at centromeric regions in *Arabidopsis*[18,19,53]. Herbicide treatment of *Arabidopsis* leads to more than 9000 DMRs of which ~6000 are dosage-dependent[17]. Both soybean root hairs and stripped roots show hypomethylation after heat stress (40°C), especially in the CHH context[16]. In rice, Pi starvation induces widespread changes in DNA methylation, especially the TEs in proximity to Pi-starvation induced genes[54]. Heavy metals such as cadmium induces DNA hypomethylation in industrial hemp (*Cannabis sativa*), clover (*Trifolium repens*), and seagrass (*Posidonia oceanica*)[55,56]. The genome of *Arabidopsis* flown onboard of the scientific satellite SJ-10 exhibited lower methylation levels, while the leaves of *Arabidopsis* grown in the International Space Station showed higher methylation levels in protein coding genes[20,21]. Together, these studies suggest that plant epigenome is plastic and can be ‘edited’ by versatile environmental cues. Future mechanistic study is important to understand how cells modulate their epigenomes to generate adaptive responses.

In *Arabidopsis*, several DRM2 interacting proteins have been identified including AGO4, RNA-directed DNA Methylation 1 (RDM1), and U2AF56 Associated Protein 56 (UAP56)[34,57–59]. In the RdDM pathway, siRNAs are loaded onto AGO4 and pair with complementary long Pol V transcripts[11]. The interaction between AGO4 and DRM2 is thought to guide DRM2 to specific genomic regions to establish *de novo* DNA methylation[34]. RDM1, also a component of the DDR complex, physically associates with both AGO4 and DRM2 and is proposed to promote the AGO4-DRM2 interaction[57]. UAP56 is a DEAD box RNA helicase and partially co-localizes with DRM2[58]. Despite some chromatin-associated properties, its function in epigenome regulation remains unclear. In rice, OsDRM2 has been reported to interact with OseIF4A (an ATP-Dependent RNA Helicase) and SDG711 (a H3K27me3 methyltransferase in PRC2 complex)[60,61]. Interestingly, all current known DRM2-interacting proteins play positive roles in facilitating DRM2-mediated DNA methylation. In contrast, multiple lines of genetic, genomic, and biochemical evidence in this study demonstrated that UVR8 inhibits DRM2 function, highlighting the first negative regulator of this plant DNA methyltransferase. Consistently, the *de novo* methyltransferase DNMT3A has been reported to interact with MeCP2, which negatively regulates the activity of DNMT3A in human[62].

UBA domains are found in many proteins involved in degradation pathways and ubiquitin-dependent signaling pathways by recognizing various ubiquitin forms including poly- and mono-ubiquitin[63]. The UBA domains of DRM2 have been reported to mediate its interactions with other proteins. For OseIF4A and SDG711, their interactions with OsDRM2 are mediated by the UBA domains[60,61]. Given that UVR8 interacts with the UBA domains, we wonder whether UBA domains serve as a platform mediating interaction with multiple proteins to regulate the complex function *in vivo*. Similar to UVR8, we indeed found that the UBA domains, but not methyltransferase domain, interact with AGO4 (Supplementary Fig. 5a). Within DRM2, UBA domains also tends to self-associate and associate with methyltransferase domain (Supplementary Fig. 5b). Consistent with this notion, the UBA domains are indispensable for DNA methylation catalyzed by DRM2 *in vivo*[34]. UBA domains are known to associate with ubiquitin, however, none of the currently known DRM2-interacting proteins have been reported to be ubiquitylated. Previously, DRM2 UBA domains were shown to bind to poly-ubiquitin chains with preference for Lys63-linked chains *in vitro*[64]. While poly-ubiquitylation is often associated with protein degradation, mono-ubiquitylation have been implicated in a variety of pathways such as endocytosis, DNA repair, and cell signaling[65]. Thus, it will be important to identify additional proteins associated with DRM2 UBA domains to further connect the DNA methylation and ubiquitylation fields.

It appears that UVR8 has a dual role on DRM2 function. In one capacity, UVR8 can inhibit the catalytic activity of DRM2 (Fig. 6d). In another capacity, UVR8 can inhibit DRM2 chromatin association (Fig. 6e). While the precise mechanism is unclear, several possibilities could account for this dual action. First, the UVR8 binding may induce a conformational change of DRM2, resulting in its dysfunction in both chromatin association and catalytic activity. Second, UVR8 binding of UBA domains may outcompete other chromatin and transcription factors and disable their association with DRM2. As discussed earlier, UBA domains are thought to be mediators of protein-protein interactions. UVR8 may either directly or indirectly via other factors inhibit DRM2 chromatin association. For example, UVR8 binding to transcription factors BES1, BIM1, MYB73/77, and WRKY36/13 repressed their association with chromatin[28–31]. While this makes sense with the chromatin binding, it raises an interesting question as to how UVR8 can inhibit the catalytic activity by binding to UBA domains. A possible mechanism is the allosteric inhibition of UVR8 on DRM2. The UBA domains may interact with the methytransferase domain in an intra-molecular or inter-molecular manner to inhibit catalytic activity. The binding of UVR8 with UBA domains further enhances this negative regulation. This is consistent with the case of DNMT3A-MeCP2, where the interaction of MeCP2 with the ADD domain of DNMT3A stabilizes DNMT3A's autoinhibitory conformation and, thus, inhibits its catalytic activity[62].

In both UVB treated Col-0 and *dd* mutant, we found that UVB could de-repress many TEs (Fig. 3). This is consistent with the idea that DNA methylation primarily represses the TEs to maintain the genome stability in plants[6,42]. UVB activates the expression of a DNA transposon *Mutator* in maize[66], consistent with our results that UVB-induced hypo DMRs are enriched in DNA transposon (Extended Data Fig. 3g). In nature, an *Arabidopsis* relative *Crucihimalaya himalaica* from Qinghai-Tibet Plateau with high levels of UVB irradiation shows LTR retrotransposons expansion shortly after the dramatic uplift and climatic change

of the Himalayas from the Late Pliocene to Pleistocene[67]. Transposon reactivation in response to stress could increase phenotypic diversity and adaptability to changing environment by transcriptional regulation of neighboring genes and by novel transposon insertions[10,68]. For example, *Capsella rubella* exhibits a wider distribution and higher phenotypic diversity accompanied with highly enriched TEs compared with its congeneric species such as *Capsella grandiflora*[69], suggesting that TE insertions can drive rapid phenotypic variation and potentially promote adaptation to changing environments. When these results are collectively reviewed along with our present findings, it is therefore likely that UVB-induced DNA methylation reduction and TE reactivation is a mechanism of plant adaption to changing local environment by promoting phenotypic and genetic diversity.

Methods

Plant materials

For *Arabidopsis thaliana,* the Columbia-0 (Col-0) ecotype was used as the background for all mutant and transgenic plants. The mutant lines used were *uvr8–6* (SALK_033468), *drm1–2 drm2–2* (*dd,* SALK_031705, SALK_150863), *cop1–6* (CS69041), and *fwa-4* (epiallele mutant). The DNA methylation reporter lines, *LUCH* and *LUCL* reporter lines[35] and *pSDC:GFP*/*cmt3*[70], have been described previously. *LUCM* is from the same batch as *LUCH* and *LUCL* but characterized in this study. Multiple mutants and reporters under mutant backgrounds (*uvr8–6 dd* (*udd*), *uvr8–6 LUCM*, *cop1–6 LUCM*) were generated by crossing and further genotyping. The transgenic lines used in this study include *UVR8-FLAG* (*35S*), *UVR8-HA* (*35S*) in Col-0 and *3F9M-DRM2*/*dd* backgrounds, *FWA* in Col-0, *dd*, *uvr8–6*, *udd*, and *UVR8-FLAG* backgrounds.

UVB treatment

The UVB treatments were performed using Philips UVB lamps TL20W/01RS for narrow band UVB (305 to 315 nm, with peak at 312 nm), and TL40W/12RS for broadband UVB (290 to 315 nm). The UVB intensity on plants was manipulated by adding plastic tape and adjusting the distance between the plants and the lamp, and was measured by a UVA/B Light Meter (SPER Scientific, model 850009). For narrowband UVB, the intensity unit of μmol m^{-2} s^{-1} was calculated approximately using the peak wavelength of 312 nm from μW/cm^2. For plants used for whole-genomic bisulfite sequencing (WGBS), RNA-sequencing, and DNA methylation reporters (*LUCM* and *pSDC:GFP cmt3*), seeds were planted on ½ MS plates with 1% sucrose and 0.7% agar. The seeds were put directly under narrowband UVB lamp with a UVB intensity of 1.5 μmol·m^{-2}·s^{-1} (~60 μW/cm^2) and 60 μmol·m^{-2}·s^{-1} of white light after stratification. For the split luciferase assay after UVB treatment, the infiltrated *N. benthamiana* leaves were treated with narrowband UVB for 30 min before fluorescence imaging. For the UVR8- and DRM2-GFP localization by UVB treatment, 7-day old homozygous transgenic seedlings on ½ MS plates were put under narrowband UVB lamp for 4 hours and then imaged with a confocal microscope (Nikon A1R). For CoIP after UVB treatment, 10-day old seedlings were put under narrowband UVB lamp for 4 hours and then directly subjected to nuclei isolating and CoIP. For ChIP-qPCR, the flowering *gDRM2-FLAG*/*dd* and *gDRM2-FLAG*/*udd* plants were treated with broadband UVB for one hour. 1.5 to two grams of flowers were collected after UVB treatment immediately. For UVB

stress treatment, 10-day old seedlings grown on ½ MS plates were treated with broadband UVB (~430 μW/cm^2) for 3.5 hours in addition to white light (~60 μmol·m^{-2}·s^{-1}) and then recovered under white light for 1 week. The plants with newly grown leaves were defined as survived plants.

Co-immunoprecipitation

Co-immunoprecipitation in *Arabidopsis* was performed with homozygous *UVR8-HA* transgenic plants in *3F9M-DRM2/dd* or Col-0 backgrounds. For CoIP after isolating nuclei, fresh 10-day old seedlings were chopped with a blade and then grinded with mortar/pestle in ice-cold Nuclei Isolating Buffer (NIB, 10 mM MES-KOH, pH5.5, 2.5 mM EDTA, 10 mM NaCl, 10 mM KCl, 0.2 M Sucrose, 0.1 mM Spermidine, 2.5 mM DTT). Then the samples were filtered through 2 layers of miracloth and centrifuged at 1000 g for 10 min at 4°C. The pellet containing nuclei was then resuspended in CoIP binding buffer (20 mM HEPES, pH 7.5, 40 mM KCl, 1 mM EDTA, 1% Triton X-100, and protease inhibitor cocktail), lysed using a Dounce tissue grinder (Sigma) and rotated at 4°C for 30 min. After centrifuging, the supernatant was incubated with 6 μl FLAG magnetic beads for one hour. The beads were then washed with CoIP wash buffer (20 mM HEPES, pH 7.5, 40 mM KCl, 1 mM EDTA, 0.1% Triton X-100) for three times, and boiled at 95°C in 1x SDS loading buffer. For Co-IP using total proteins, 4-week-old rosette leaves were ground to a fine powder using a mortar and pestle in liquid nitrogen. Total proteins were then extracted by grinding the powder with CoIP buffer, lysis with Dounce tissue grinder (Sigma) and incubating with rotation at 4°C for 30 min. After centrifuging, the supernatant was filtered through a 0.45 μm membrane and incubated with 10 μl FLAG magnetic beads for one hour. After washing with CoIP wash buffer for five times, beads were boiled at 95°C in 1x SDS loading buffer. For Co-IP in *N. benthamiana*, the leaves were co-infiltrated with Agrobacterium carrying UVR8-HA and DRM2-FLAG. Total proteins were extracted with 2x extraction buffer and then immunoprecipitated with 5 μl FLAG beads for one hour at 4°C. After washing with the same buffer five times, the beads were boiled in 1x SDS loading buffer.

Immunoblotting

Protein samples were run on SDS-PAGE gels and transferred to nitrocellulose membranes. The membranes were blocked with 5% non-fat milk, rinsed with TBST, and then incubated with primary and/or secondary antibodies. The primary antibodies used were anti-FLAG-HRP (Sigma, 1:5000), anti-HA-HRP (Roche, 1:5000), anti-GFP (Roche, 1:1000), anti-actin (Proteintech, 1:5000), anti-tubulin (Servicebio, 1:5000), and anti-H3 (Abcam, 1:1000). All antibodies were in 3% BSA in 1x TBST buffer. Chemiluminescence images were taken after adding ECL substrate with ImageQuant LAS4000 (GE).

Split luciferase and luciferase imaging

For split luciferase assays, Agrobacterium carrying nLuc and cLuc plasmids were cultured in liquid LB media, resuspended to optical density at 600 nm (OD_{600}) ~0.02 in buffer (10 mM MES, 10 mM $MgCl_2$, 200 μM acetosyringone), and then mixed with equal volume. The Agrobacterium suspensions were infiltrated into the leaves of 3- to 5-week old *N. benthamiana*. After 36–48 hours, the leaves were sprayed with 2 mM luciferin (Promega) in 0.01% Triton X-100 solution and kept in darkness for 5 min. Chemiluminescence images

were then taken with a 5 min exposure. For luciferase imaging in *Arabidopsis*, 6- or 7-day old seedlings on ½ MS plates were sprayed with 1 mM luciferin. All images were pseudo-colored with ImageStudio (LI-COR) to reveal the signal intensity. Quantification of luciferase signal was done with ImageJ (NIH).

Bimolecular fluorescence complementation (BIFC) and confocal microscopy

The BIFC protein-protein interaction assay was performed in *N. benthamiana* leaves. Agrobacterium carrying nYFP and cYFP series plasmids were infiltrated to *N. benthamiana* leaves using a similar method as split luciferase assay. After 36–48 hours, the infiltrated leaves were visualized and imaged with confocal laser fluorescence microscopy (Nikon A1R). For subcellular localization of GFP and mCherry reporters in *N. benthamiana*, similar methods were performed. For localization of DRM2-GFP in *Arabidopsis*, the root tip and leaves were used. The excitation wavelengths for YFP/GFP and mCherry were 488 nm and 561 nm, respectively, and the emission wavelengths for YFP/GFP and mCherry were 500–550 nm and 570–620 nm, respectively. All confocal images were exported as TIFF images with single channel and merged multiple channels.

Quantitative real-time PCR analysis

For RT-qPCR, plant total RNA was extracted using Ambion PureLink RNA Mini Kit (Invitrogen). The first strand cDNA was then synthesized from 2 μg of the extracted total RNA using anchored oligodT_{18}VN and random hexamer primers, and SuperScript III (Invitrogen) or ProtoScript II (NEB) reverse transcriptases. For Chop-qPCR, plant genomic DNA was extracted with the CTAB method[71]. Equal amount of genomic DNA was then digested with McrBC and HaeIII (NEB) for 6 hours at 37°C. For ChIP-qPCR, 0.5 μl of immunoprecipitated DNA was used as template. The quantitative real-time PCR was performed in triplicates using SYBR Green qPCR Master Mix (Vazyme) and a Bio-Rad CFX96 C1000 Real-Time system. The gene expression levels in RT-qPCR were normalized against wild type control and internal control *ACT7* or an *U-box* gene (At5g15400). The relative methylation levels of Chop-qPCR were normalized to uncut control. The relative enrichment of each locus in ChIP was normalized to Col-0.

DNA methyltransferase activity assay

The methyltransferase assay was carried out at 30°C for one hour in a total volume of 25 μl containing 1.5 μl of S-adenosyl-l-[methyl-^{3}H] methionine (SAM) (14.4 Ci/mmol; PerkinElmer), 1.5 μl substrate DNA (12 repeats of TAC, annealed to form dsDNA, 15 μM), and 0.2 μM AtDRM2 full length (59–626) or DRM2 methyltransferase (DRM2^{CAT}, 269–626) proteins, 1 μM His-tag UVR8 or GFP proteins in assay buffer (20 mM MOPS [pH 7.0], 1 mM DTT, 5 mM EDTA, 200 μg/ml BSA, and 5% glycerol). The reactions were stopped by adding 1 μl of cold SAM (NEB). A total of 11 μl from each reaction was applied onto DEAE Filtermat (PerkinElmer,1450–522) and washed two times with 200 mM ammonium bicarbonate, two times with water, and two times with ethanol. The paper was dried and placed into 4 mL of liquid scintillation cocktail (Fisher Scientific) and the activity was measured by Liquid Scintillation Analyzer (PerkinElmer, Tri-Carb 2910 TR).

Chromatin immunoprecipitation (ChIP)

For DRM2-FLAG ChIP, flowers from *gDRM2-FLAG/dd* and *gDRM2-FLAG/udd* transgenic plants were used. For UVB treated samples, plants were treated with broadband UVB for one hour. 1–2 g of flowers were ground into fine powders in liquid nitrogen with a mortar and pestle. The powder was then crosslinked in nuclei isolation buffer (10 mM HEPES, pH 8.0, 1 M sucrose, 5 mM KCl, 5 mM $MgCl_2$, 5 mM EDTA, 0.6% Triton X-100, 0.4 mM PMSF, and protease inhibitor cocktail) with 1% formaldehyde for 15 minutes at room temperature. Cross-linking was stopped by adding 125 mM glycine and shaking for 15 minutes. The homogenate was filtered through two layers of Miracloth (Millipore) and centrifuged at 3000g for 20 min at 4°C. The pellet was resuspended with ChIP buffer 2 (10 mM Tris-HCl, pH 8.0, 0.25 M sucrose, 10 mM $MgCl_2$, 1% Triton X-100, 1 mM EDTA, 5 mM β-mercaptoethanol, and protease inhibitor cocktail tablet) and re-pelleted by centrifuging. The pellet was resuspended in MNase buffer (50 mM Tris-HCl, pH7.5, 50 mM NaCl, 5 mM $MgCl_2$, 5 mM $CaCl_2$, 10% glycerol, 0.1% NP50, 0.1 mM PMSF, and protease inhibitor cocktail), and sheared by sonication using a Diagenome sonicator (Covaris) for 10 min and MNase digestion for 20 min. After centrifugation at 12000 rpm for 10min, 300 ng human H3.2-FLAG-HA chromatin was added (spiked-in) to the supernatant. The chromatin-containing supernatant was incubated with 30 μl of FLAG-M2 (Sigma) beads overnight with rotation at 4°C. The beads were sequentially washed with MNase buffer, high-salt MNase buffer (300 mM NaCl), LiCl buffer (250 mM LiCl, 1% NP-40, 1% sodium deoxycholate, 1 mM EDTA, and 10 mM Tris-HCl, pH 8), and TE buffer (10 mM Tris-HCl, pH 8, and 1 mM EDTA). The DNA-protein complex was then eluted with ChIP elution buffer (1% SDS and 0.1 M $NaHCO_3$) and reverse cross-linked at 65°C for over 6 hours. After sequential RNase and proteinase K treatments, DNA was purified using the standard phenol-chloroform method and used for further qPCR analyses.

Bisulfite sequencing

For whole genome bisulfite sequencing, seeds of Col-0 and a *UVR8-OX* transgenic line were planted on ½ MS medium, treated with or without narrowband UVB (~50 μW/cm^2) for 10 days. Genomic DNA was then extracted from the whole seedlings using a DNeasy Plant Mini Kit (Qiagen). The genomic DNA was fragmented to a mean size of 100–300 bp by sonication using a Covaris S220 focused-ultrasonicator (Covaris), followed by end-repair, 3'-end adenylation and methylated adaptor ligation using Illumina TruSeq DNA kit (Illumina). Then bisulfite conversion was performed using a Zymo EZ DNA Methylation-Lightning kit (Zymo Research). The bisulfite-converted, adaptor-ligated DNA was enriched by PCR for 12–15 cycles using KAPA HiFi HotStart Uracil+ Kit (KAPA Biosystems), purified with Agencourt beads (NuGen) and quantified by Qubit HS dsDNA kit (Life Technologies). The integrity of the sequencing library was tested by Agilent 2100. The libraries were sequenced by 50 bp single-end method on a HiSeq4000 platform at NUcore sequencing center in Northwestern University (Chicago, IL, USA).

For bisulfite-Sanger sequencing, the genomic DNA was bisulfite converted using an EZ DNA Methylation-Gold kit (Zymo Research). PCR was then performed using a MyTaq Mix (Bioline). The PCR products were purified from agarose gels and ligated to pCR2.1 using a

TOPO TA Cloning kit (Thermo Fisher Scientific). 10 to 19 clones were sequenced (Genewiz LLC) and analyzed with Kismeth (http://katahdin.mssm.edu/kismeth/revpage.pl).

RNA-sequencing

For RNA-sequencing, total RNA was extracted using Ambion PureLink RNA Mini Kit (Invitrogen) and treated with DNase I. RNA-seq libraries were constructed using a TruSeq RNA Library Preparation Kit (Illumina, RS-122–2002). In brief, mRNA was purified with RNA purification beads, and fragmented with Elute, Primer, Fragment Mix. Later, ds-cDNA was synthesized with SuperScript II (Invitrogen) followed by second strand synthesis. End-repair, 3'-end adenylation, ligation of adaptors, and PCR amplification for 12 cycles were then performed. Libraries were sequenced on a HiSeq 2500 sequencing system (Illumina) in the UW-Madison Biotechnology Center. Two biological replicates were performed for RNA-seq.

High throughput sequencing data analysis

Bisulfite-seq reads were aligned to the TAIR10 genome using BSmap version 2.9[72]. Reads were filtered for < 5 N, Bisulfite-seq reads were filtered using Trimmomatic version 0.39[73] and then aligned to the TAIR10 genome using BSmap version 2.90. For metaplots, we calculated average methylation level in CG, CHG, CHH context with bedtools[74] and plot with R software (https://www.r-project.org/). For DMR calling, we used both MethylKit package[75] and Fisher's exact test to call DMRs and the overlapped DMRs were then used for subsequent analysis.

For RNA-seq analysis, we firstly filtered reads with Trimmomatic version 0.39[73] and then aligned to the TAIR10 genome using HISAT2 (version 2.0.0-beta)[76]. The alignments were then filtered with a bash code to keep the uniquely mapped reads. The quantification of gene expression and the identification of DEGs were performed with Cufflinks v2.2.1[77]. Heat map was made using Heatmapper (http://www.heatmapper.ca/expression/). The snapshot of track data were made using IGV browser.

Quantification, statistical analysis, and reproducibility

Quantification of immunoblots and luciferase were carried out using ImageStudio and Image J. Statistical analyses were carried out using Excel, GraphPad Prism, and R. Data are presented as mean ± SD or mean ± SEM as indicated. All statistical test used was two-sided. For the immunoblots and micrographs, at least two independent experiments were repeated with similar results.

Data availability

All WGBS and RNA-seq data produced during this study were deposited into Gene Expression Omnibus under accession number GSE132944.

Extended Data

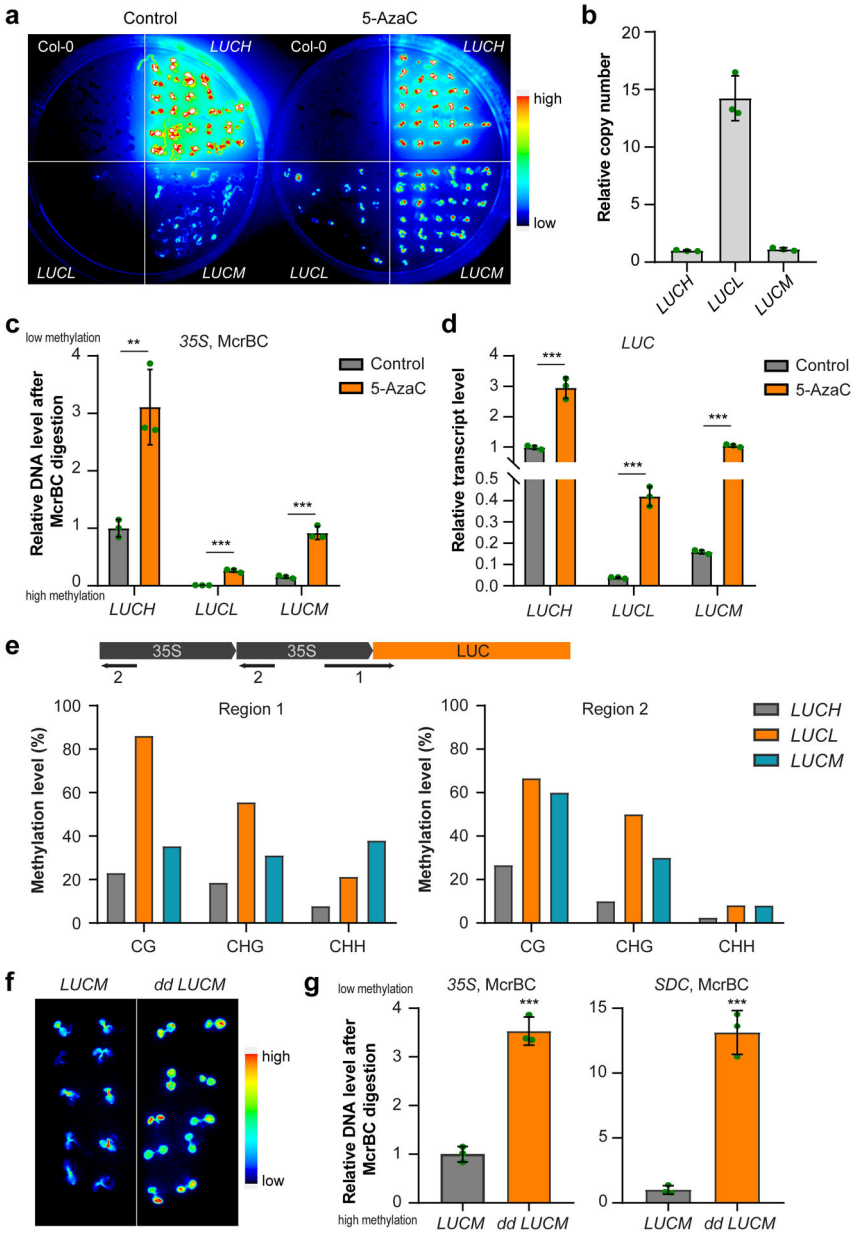

Extended Data Fig. 1. Characterization of *LUCM* reporter line

a, Luciferase images of Col-0 and three *d35S:LUC* reporter lines treated with DNA methylation inhibitor 5-Azacytidine (5-AzaC, 100 μM) for 7 days. *LUCL* and *LUCH* are previously reported (ref[35]) low and high *LUC* expressing lines, respectively. **b,** Copy number of *35S-LUC* transgene in *LUCL*, *LUCH*, and *LUCM* lines revealed by qPCR of *LUC* using genomic DNA. Data is mean ± SD. **c,** McrBC-qPCR based DNA methylation assay of *35S* promoter regions in *LUCL*, *LUCH*, and *LUCM* lines. Low amplification represents high DNA methylation level. Data is mean ± SD. **, p<0.01; ***, p<0.001 by Student's t-test. **d,** Relative transcript level of *LUC* gene in *LUCL*, *LUCH*, and *LUCM* lines. Data is mean ± SD. ***, p<0.001 by Student's t-test. **e,** Bisulfite sequencing of indicated regions (1 and 2)

in *LUCL*, *LUCH*, and *LUCM* lines. **f,** Luciferase images of 5-d old *LUCM* and *dd LCUM* (*drm1 drm2 LUCM*) seedlings. **g,** McrBC-qPCR based DNA methylation assay of *35S* promoter regions. *SDC* serves as a control for *dd*. Data is mean ± SD. ***, p<0.001 by Student's t-test.

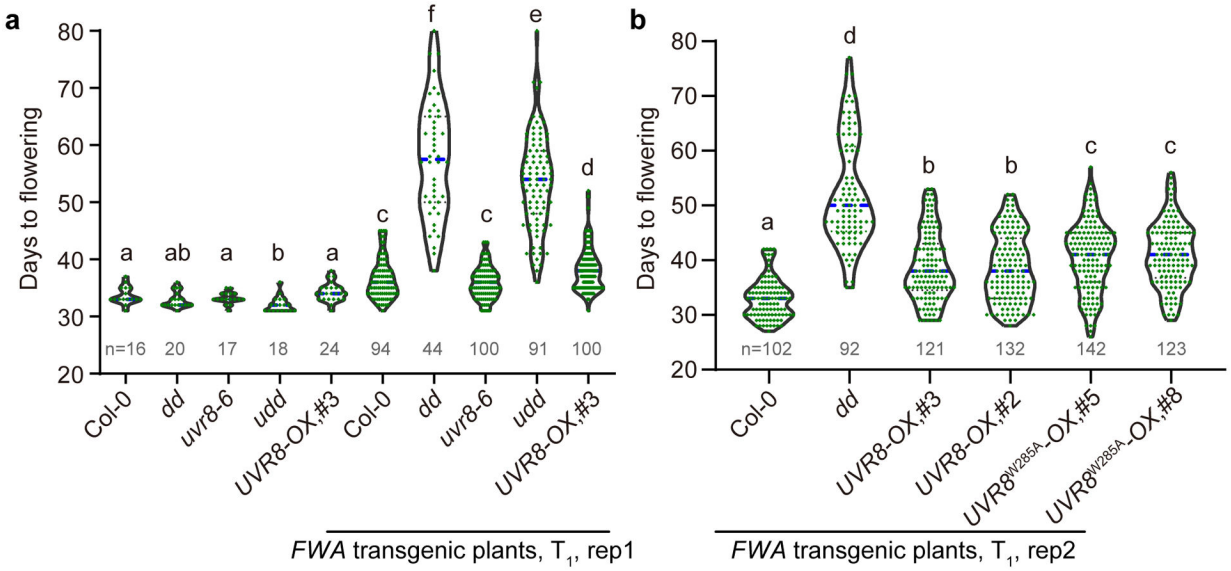

Extended Data Fig. 2. Flowering phenotypes of *FWA* transgenic plants.

a and **b**, The flowering time of *FWA* transgenic T_1 plants from two replicates with replicate 1 in (**a**) and replicate 2 in (**b**). Indicated genotypes were transformed with *FWA* transgene and the flowering time of positive Basta-resistant T_1 transformants were counted. The non-transformed plants serve as controls. The number of plants is indicated by n. *dd*, *drm1 drm2*; *udd*, *uvr8–6 drm1 drm2*; *UVR8-OX*, *35S:UVR8-FLAG* overexpression lines (#3 and #2); *UVR8^{W285A}-OX*, *35S:UVR8^{W285A}-FLAG* overexpression lines (#5 and #8). The blue dash line indicates median. Each dot represents a single plant. Significantly different (p<0.05 by Student's t-test) groups are labelled with different letters.

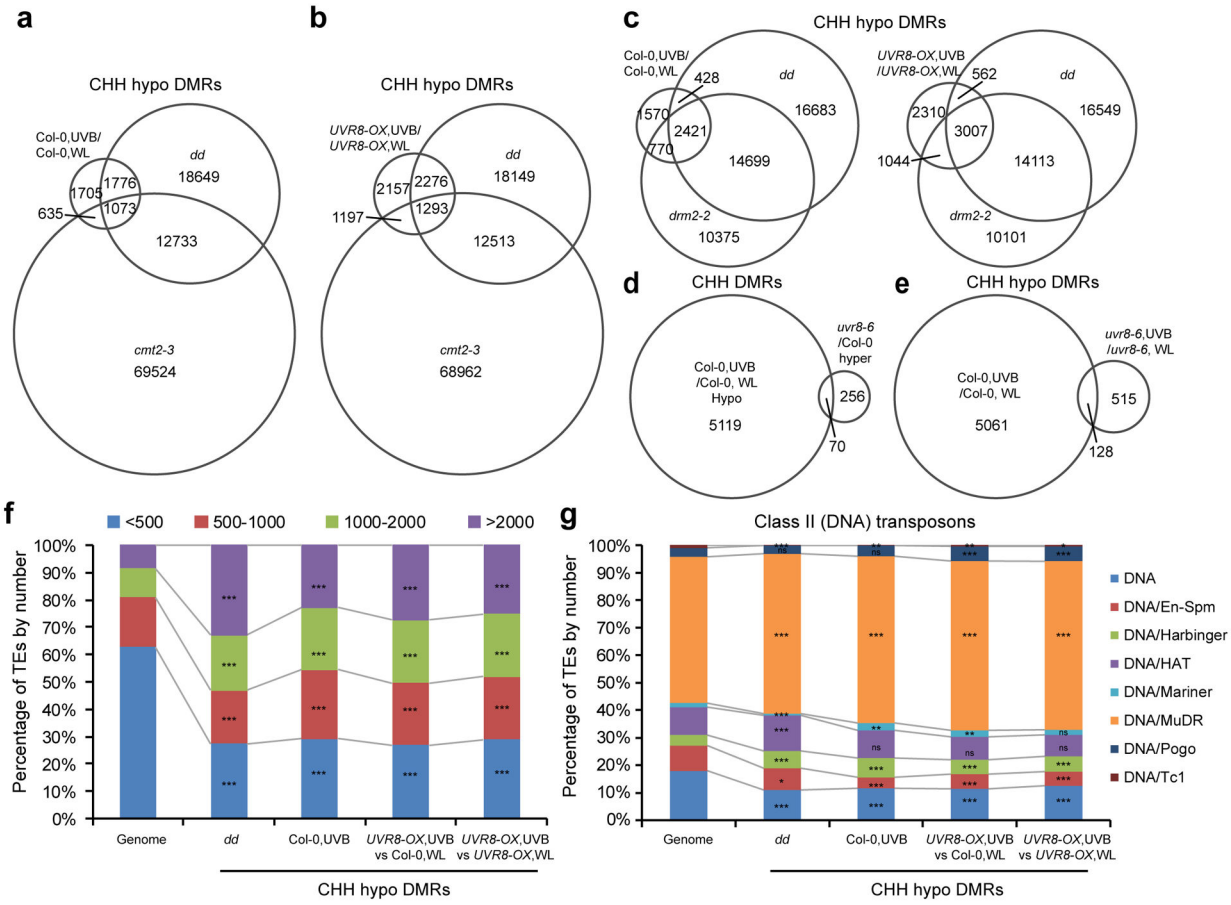

Extended Data Fig. 3. Analysis of UVB-induced differentially methylated regions

a and **b,** Venn diagrams showing the overlap of CHH hypo differential methylation regions (DMRs) among *drm1 drm2* (*dd*), *cmt2–3*, and UVB-induced DMRs in Col-0 (**a**) and *UVR8-OX* (**b**). Data of *dd* and *cmt2–3* are from ref[78]. **c,** Venn diagrams showing the overlap of CHH hypo DMRs among UVB-treated Col-0 (left) or *UVR8-OX* (right), *dd*, and *drm2–2* mutant. Data of *drm2–2* is from ref[79]. **d,** Venn diagrams showing the overlap of UVB-induced CHH hypo DMRs in Col-0 with hyper DMRs in *uvr8–6* mutant. **e**, Venn diagrams showing the overlap of UVB-induced CHH hypo DMRs in Col-0 and *uvr8–6.* **f**, The enrichment of TEs containing CHH hypo DMRs based on length. ***, p<0.001 by Fisher's exact test. **g,** The enrichment of Class II (DNA) TEs containing CHH hypo DMRs. ***, p<0.001; **, p<0.01; *, p<0.05; ns, not significant by Fisher's exact test.

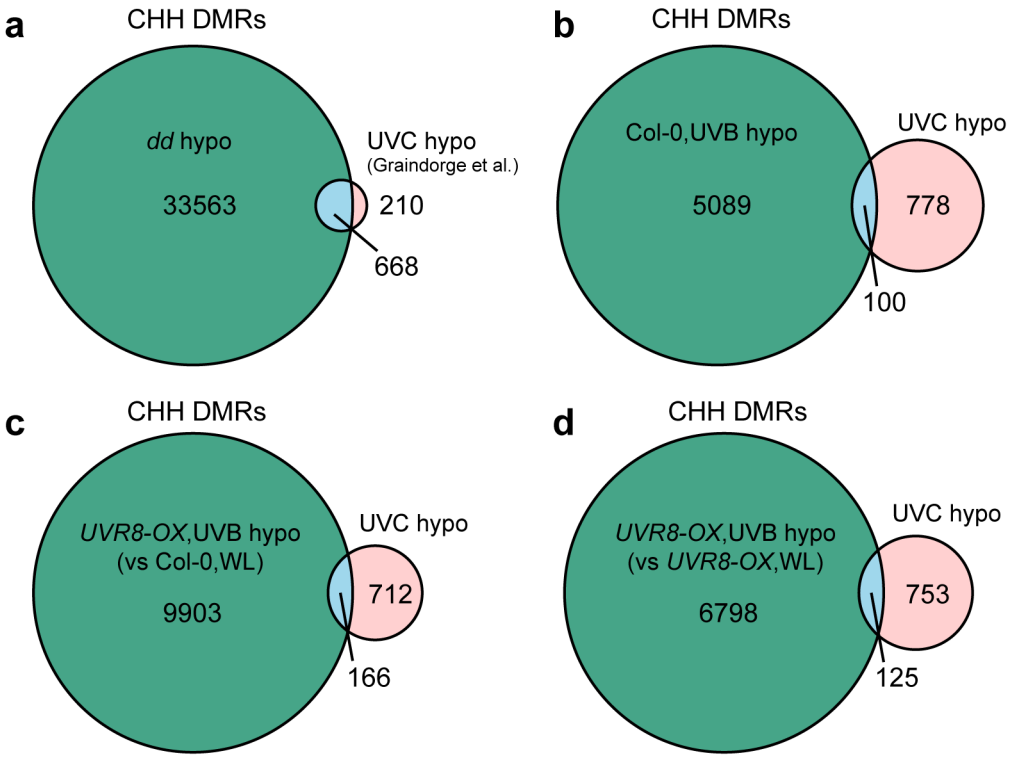

Extended Data Fig. 4. Comparison of UVB- and UVC-induced DMRs

a, Overlapping of CHH hypo DMRs by UVC treated Col-0 (compared to Col-0 without treatment) and *drm1 drm2* (*dd*). The UVC-induced DMRs are from ref[41] (GSE132750). **b**, Overlapping of UVB- and UVC-induced CHH hypo DMRs in Col-0. **c**, Overlapping of CHH hypo DMRs of UVB treated *UVR8-OX* (compared with Col-0,WL) and UVC. **d**, Overlapping of CHH hypo DMRs of UVB treated *UVR8-OX* (compared with *UVR8-OX*,WL) and UVC.

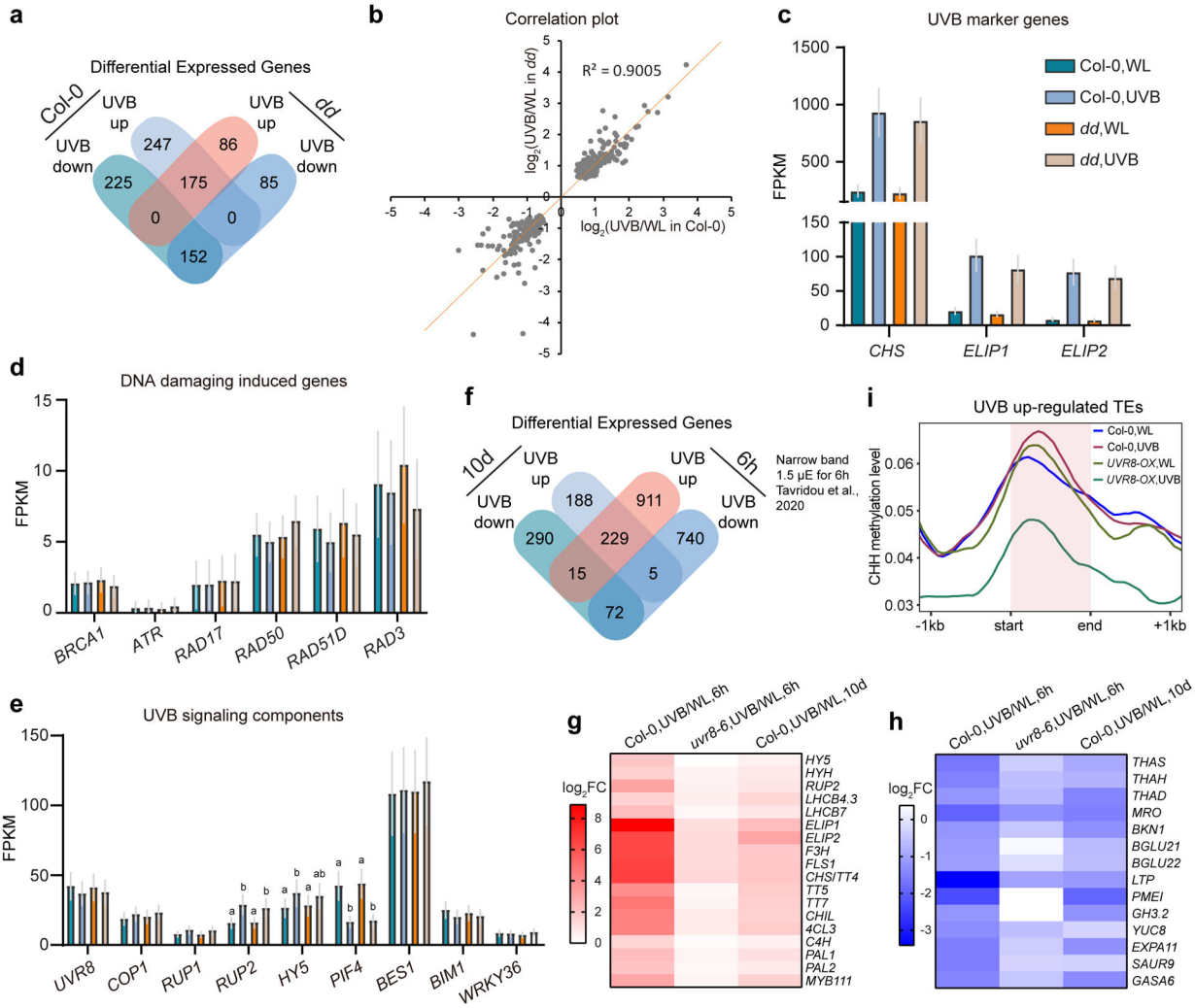

Extended Data Fig. 5. Differential expressed genes (DEG) induced by UVB

a, Venn diagram showing the overlapping of DEGs induced by UVB in Col-0 and *drm1 drm2* (*dd*). **b**, Correlation plot showing the expression level change (log_2FC) of common UVB-responsive DEGs in Col-0 and *dd* (n=327). **c**, Expression levels of marker genes, which are up-regulated by UVB, in Col-0 and *dd*. Data is mean with 95% confidence interval. **d**, Expression levels of DNA-damaging induced genes in Col-0 and *dd*. Data is mean with 95% confidence interval. **e**, Expression levels of genes in UVB-signaling pathway. Data is mean with 95% confidence interval. Different letters denote significant differences ($p<0.05$ by Student's t-test) among samples. **f**, Venn diagram showing the overlapping of DEGs induced by long-term (10d, this study) and short-term (6h, ref[80]) UVB treatment in Col-0. **g** and **h**, Heat map showing the expression of several UVB up-regulated (**g**) and down-regulated (**h**) DEGs in both long-term and short-term UVB treatment. **i**, Metaplots showing the CHH methylation level of UVB up-regulated TEs (n=269). Data of 1 kb upstream and downstream of the TE body are shown.

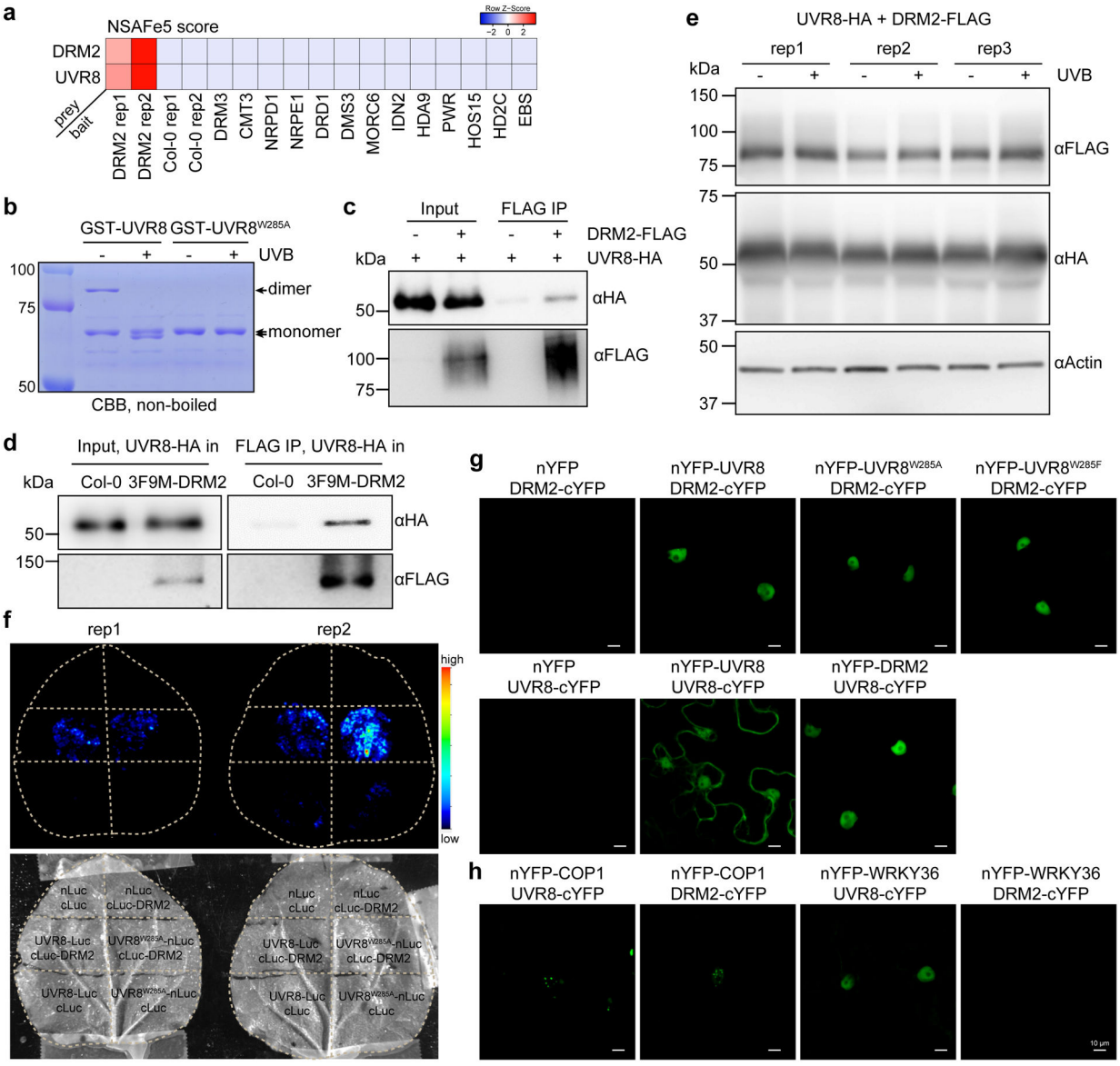

Extended Data Fig. 6. DRM2 interacts with UVR8 and its active form UVR8^{W285A}

a, Heatmap showing the NSAF score (an indicator of normalized spectral abundance factor) of UVR8 and DRM2 in various immunoprecipitation-mass spectrometry (IP-MS) experiments. The IP-MS data of DRM2 is from ref[34], DRM3 and NRPE1 are from ref[81], CMT3 is from ref[82], DRD1 and DMS3 are from ref[83], MORC6 is from ref[70], IDN2 is from ref[84], HDA9 and PWR are from ref[85], HOS15 is from ref[86], HD2C is from ref[87], EBS is from ref[88]. **b,** Coomassie bright blue staining of non-boiled GST-UVR8 proteins on SDS-PAGE. The GST-UVR8^{W285A} proteins serve as control for monomer. **c,** Co-immunoprecipitation of UVR8 and DRM2 with FLAG beads from *N. benthamiana* leaves co-expressing UVR8-HA and DRM2-FLAG. **d**, Co-immunoprecipitation of UVR8 and DRM2 with FLAG beads from transgenic *Arabidopsis* plants co-expressing UVR8-HA and 3F9M-DRM2. UVR8-HA in Col-0 serves as a control. **e,** Immunoblots showing protein levels with or without UVB treatment. The ±UVB set-up is the same as that in Fig. 4g. Actin

serves as an internal control. **f**, Split luciferase assay showing the interaction between DRM2 and UVR8^{W285A}. The indicated constructs were co-expressed in *N. benthamiana* leaves and imaged after spraying with the luciferin. nLuc- and cLuc-only vectors serve as negative controls. Two biological replicates are shown. **g,** Bimolecular fluorescence complementation (BIFC) assays in *N. benthamiana* leaves showing the interaction between DRM2 and different forms of UVR8. Scale bar, 10 μm. **h,** BIFC assays co-expressing indicated proteins in *N. benthamiana* leaves. Scale bar, 10 μm.

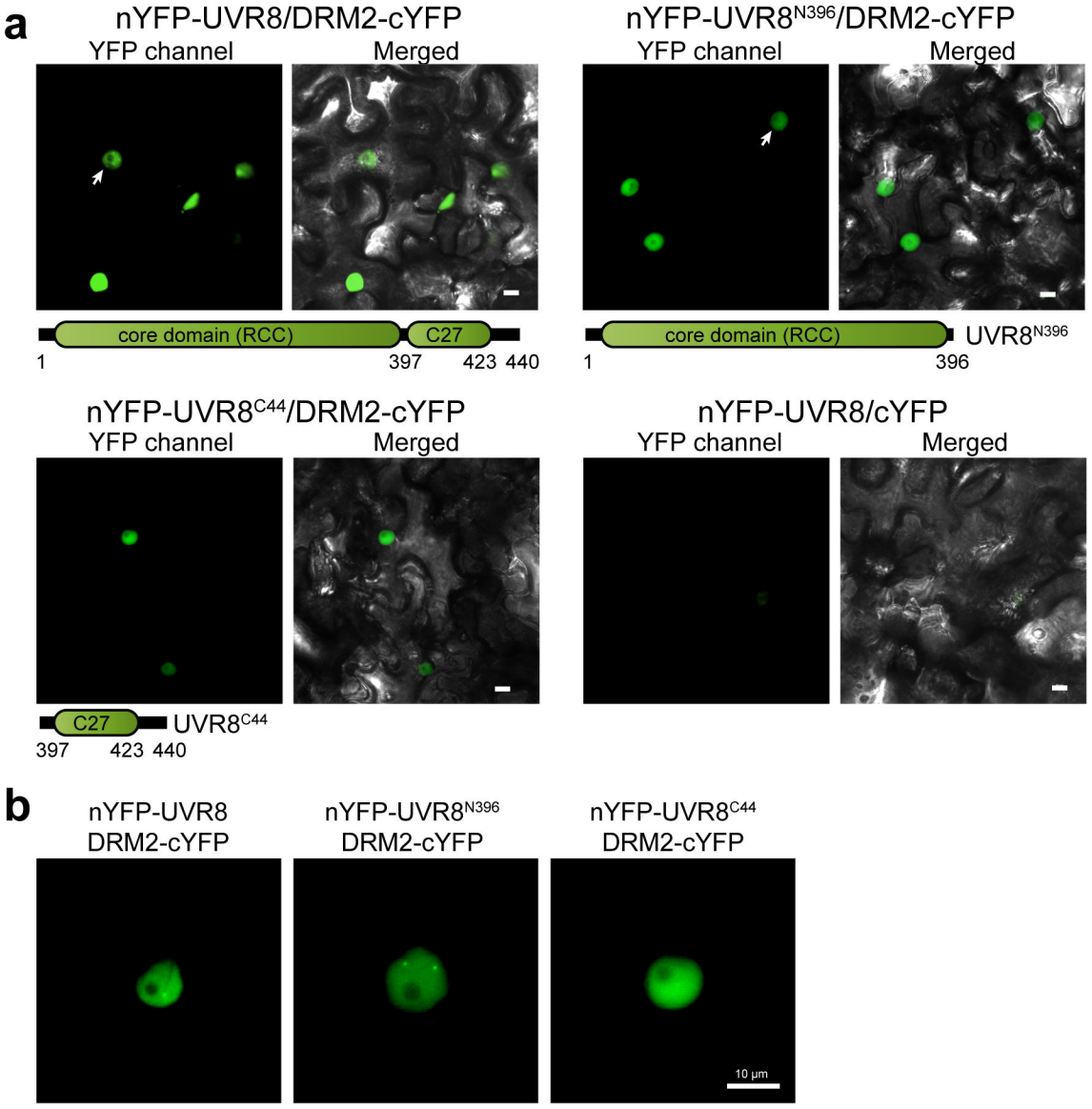

Extended Data Fig. 7. DRM2 interacts with both the core domain and the C-terminus of UVR8

a, Bimolecular fluorescence complementation (BIFC) assays in *N. benthamiana* leaves. nYFP-fused full length UVR8, UVR8 core domain (UVR8^{N396}), and C-terminus (UVR8^{C44}) were co-expressed with DRM2-cYFP. The arrow indicates the nuclei showing

nuclear bodies. Scale bar, 10 μm. **b**, Magnified images showing the interaction of UVR8-DRM2, UVR8^{N396}-DRM2 in nuclear bodies. Scale bar, 10 μm.

Supplementary Material

Refer to Web version on PubMed Central for supplementary material.

Acknowledgements

We thank Steven Jacobsen (UCLA) for *pSDC:GFP/cmt3* and Xuemei Chen (UC Riverside) for *d35S:LUC* reporter lines. We thank Zhong lab members (Adeline Ding, Sarah Leichter, and Ray Scheid) for comments on the manuscript. This work was supported by NIH (R35GM124806) and USDA (Hatch 1012915) to XZ and NIH (1R35GM119721) to JS. JJ was supported by Initiative Postdocs Supporting Program (BX201600066).

References

1. Pikaard CS & Scheid OM Epigenetic regulation in plants. Cold Spring Harb. Perspect. Biol 6, a019315 (2014). [PubMed: 25452385]
2. Schübeler D Function and information content of DNA methylation. Nature 517, 321 (2015). [PubMed: 25592537]
3. Heyn H & Esteller M An adenine code for DNA: A second life for N6-methyladenine. Cell 161, 710–713 (2015). [PubMed: 25936836]
4. Springer NM & Schmitz RJ Exploiting induced and natural epigenetic variation for crop improvement. Nat. Rev. Genet 18, 563–575 (2017). [PubMed: 28669983]
5. Bewick AJ & Schmitz RJ Gene body DNA methylation in plants. Curr. Opin. Plant Biol 36, 103–110 (2017). [PubMed: 28258985]
6. Zhang H, Lang Z & Zhu JK Dynamics and function of DNA methylation in plants. Nat. Rev. Mol. Cell Biol 19, 489–506 (2018). [PubMed: 29784956]
7. Matzke MA, Kanno T & Matzke AJMM RNA-Directed DNA Methylation: The Evolution of a Complex Epigenetic Pathway in Flowering Plants. Annu. Rev. Plant Biol 66, 243–267 (2015). [PubMed: 25494460]
8. Zemach A et al. The arabidopsis nucleosome remodeler DDM1 allows DNA methyltransferases to access H1-containing heterochromatin. Cell 153, 193–205 (2013). [PubMed: 23540698]
9. Stroud H et al. Non-CG methylation patterns shape the epigenetic landscape in Arabidopsis. Nat. Struct. Mol. Biol 21, 64–72 (2014). [PubMed: 24336224]
10. Matzke MA & Mosher RA RNA-directed DNA methylation: An epigenetic pathway of increasing complexity. Nat. Rev. Genet 15, 394–408 (2014). [PubMed: 24805120]
11. Borges F & Martienssen RA The expanding world of small RNAs in plants. Nat. Rev. Mol. Cell Biol 16, 727–741 (2015). [PubMed: 26530390]
12. Farlik M et al. Resource DNA Methylation Dynamics of Human Hematopoietic Stem Cell Differentiation Resource DNA Methylation Dynamics of Human Hematopoietic Stem Cell Differentiation. 808–822 (2016). doi:10.1016/j.stem.2016.10.019
13. Bergman Y & Cedar H DNA methylation dynamics in health and disease. 20, 274–281 (2013).
14. Dominguez-Salas P et al. Maternal nutrition at conception modulates DNA methylation of human metastable epialleles. Nat. Commun 5, 3746 (2014). [PubMed: 24781383]
15. Kawakatsu T et al. Unique cell-type-specific patterns of DNA methylation in the root meristem. Nat. Plants 2, 16058 (2016). [PubMed: 27243651]
16. Hossain MS et al. Divergent cytosine DNA methylation patterns in single-cell, soybean root hairs. New Phytol. 214, 808–819 (2017). [PubMed: 28106918]
17. Kim G et al. Herbicide injury induces DNA methylome alterations in Arabidopsis. PeerJ 5, e3560 (2017). [PubMed: 28740750]
18. Dowen RH et al. Widespread dynamic DNA methylation in response to biotic stress. Proc. Natl. Acad. Sci. U. S. A 109, E2183–E2191 (2012). [PubMed: 22733782]

19. Yu A et al. Dynamics and biological relevance of DNA demethylation in Arabidopsis antibacterial defense. Proc. Natl. Acad. Sci. U. S. A 110, 2389–2394 (2013). [PubMed: 23335630]
20. Xu P, Chen H, Jin J & Cai W Single-base resolution methylome analysis shows epigenetic changes in Arabidopsis seedlings exposed to microgravity spaceflight conditions on board the SJ-10 recoverable satellite. npj Microgravity 4, 1–11 (2018). [PubMed: 29354685]
21. Zhou M, Sng NJ, LeFrois CE, Paul A-LL & Ferl RJ Epigenomics in an extraterrestrial environment: Organ-specific alteration of DNA methylation and gene expression elicited by spaceflight in Arabidopsis thaliana. BMC Genomics 20, 1–17 (2019). [PubMed: 30606130]
22. Robson TM et al. A perspective on ecologically relevant plant-UV research and its practical application. Photochem. Photobiol. Sci 18, 970–988 (2019). [PubMed: 30720036]
23. Yin R & Ulm R How plants cope with UV-B: from perception to response. Curr. Opin. Plant Biol 37, 42–48 (2017). [PubMed: 28411583]
24. Rizzini L et al. Perception of UV-B by the Arabidopsis UVR8 protein. Science 332, 103–106 (2011). [PubMed: 21454788]
25. Wu D et al. Structural basis of ultraviolet-B perception by UVR8. Nature 484, 214–219 (2012). [PubMed: 22388820]
26. Kaiserli E & Jenkins GI UV-B Promotes Rapid Nuclear Translocation of the Arabidopsis UV-B Specific Signaling Component UVR8 and Activates Its Function in the Nucleus. Plant Cell 19, 2662–2673 (2007). [PubMed: 17720867]
27. Heijde M & Ulm R Reversion of the Arabidopsis UV-B photoreceptor UVR8 to the homodimeric ground state. Proc. Natl. Acad. Sci. U. S. A 110, 1113–1118 (2013). [PubMed: 23277547]
28. Liu H et al. UVR8 Interacts with BES1 and BIM1 to Regulate Transcription and Photomorphogenesis in Arabidopsis. Dev. Cell 44, 512–523 (2018). [PubMed: 29398622]
29. Yang Y et al. UVR8 interacts with WRKY36 to regulate HY5 transcription and hypocotyl elongation in Arabidopsis. Nat. Plants 4, 98–107 (2018). [PubMed: 29379156]
30. Yang Y et al. UV-B photoreceptor UVR 8 interacts with MYB73/MYB77 to regulate auxin responses and lateral root development. EMBO J. 39, e101928 (2020). [PubMed: 31777974]
31. Qian C et al. Coordinated Transcriptional Regulation by the UV-B Photoreceptor and Multiple Transcription Factors for Plant UV-B Responses. Mol. Plant (2020). doi:10.1016/j.molp.2020.02.015
32. Rius SP, Emiliani J & Casati P P1 Epigenetic Regulation in Leaves of High Altitude Maize Landraces: Effect of UV-B Radiation. Front. Plant Sci 7, 1–13 (2016). [PubMed: 26858731]
33. Mishra A et al. Genetic differences and aberrant methylation in the apelin system predict the risk of high-altitude pulmonary edema. Proc. Natl. Acad. Sci 112, 6134–6139 (2015). [PubMed: 25918383]
34. Zhong X et al. Molecular mechanism of action of plant DRM de novo DNA methyltransferases. Cell 157, 1050–1060 (2014). [PubMed: 24855943]
35. Dinh TT et al. Generation of a luciferase-based reporter for CHH and CG DNA methylation in Arabidopsis thaliana. Silence 4, 1 (2013). [PubMed: 23561294]
36. Henderson IR & Jacobsen SE Tandem repeats upstream of the Arabidopsis endogene SDC recruit non-CG DNA methylation and initiate siRNA spreading. Genes Dev. 22, 1597–1606 (2008). [PubMed: 18559476]
37. McNellis TW, Torii KU & Deng X-W Expression of an N-terminal fragment of COP1 confers a dominant-negative effect on light-regulated seedling development in Arabidopsis. Plant Cell 8, 1491–1503 (1996). [PubMed: 8837504]
38. Chan SWL, Zhang X, Bernatavichute YV & Jacobsen SE Two-step recruitment of RNA-directed DNA methylation to tandem repeats. PLoS Biol. 4, 1923–1933 (2006).
39. Heijde M et al. Constitutively active UVR8 photoreceptor variant in Arabidopsis. Proc. Natl. Acad. Sci. U. S. A 110, 20326–20331 (2013). [PubMed: 24277841]
40. Zilberman D, Cao X & Jacobsen SE ARGONAUTE4 control of locus-specific siRNA accumulation and DNA and histone methylation. Science 299, 716–719 (2003). [PubMed: 12522258]

41. Graindorge S, Cognat V, Berens PJ, Mutterer J & Molinier J Photodamage repair pathways contribute to the accurate maintenance of the DNA methylome landscape upon UV exposure. PLoS Genetics 15, (2019).
42. Slotkin RK & Martienssen R Transposable elements and the epigenetic regulation of the genome. Nat. Rev. Genet 8, 272–285 (2007). [PubMed: 17363976]
43. Cao X et al. Conserved plant genes with similarity to mammalian de novo DNA methyltransferases. 97, 4979–4984 (2000).
44. Yin R, Arongaus AB, Binkert M & Ulm R Two Distinct Domains of the UVR8 Photoreceptor Interact with COP1 to Initiate UV-B Signaling in Arabidopsis. Plant Cell Online 27, 202–213 (2015).
45. Li CF et al. Dynamic regulation of ARGONAUTE4 within multiple nuclear bodies in Arabidopsis thaliana. PLoS Genet. 4, e27 (2008). [PubMed: 18266474]
46. Borg-Karlson A-K, Ohlsson AB, Berglund T, Segerfeldt P & Lindström A UV -B Exposure of Indoor-Grown Picea abies Seedlings Causes an Epigenetic Effect and Selective Emission of Terpenes. Zeitschrift für Naturforsch. C 68, 139–147 (2013).
47. Pandey N & Pandey-Rai S Deciphering UV-B-induced variation in DNA methylation pattern and its influence on regulation of DBR2 expression in Artemisia annua L. Planta 242, 869–879 (2015). [PubMed: 25998525]
48. Qüesta JI, Walbot V & Casati P Mutator transposon activation after UV-B involves chromatin remodeling. Epigenetics 5, 352–363 (2010). [PubMed: 20421734]
49. Lang-Mladek C et al. Transgenerational inheritance and resetting of stress-induced loss of epigenetic gene silencing in arabidopsis. Mol. Plant 3, 594–602 (2010). [PubMed: 20410255]
50. Marfil C et al. Changes in grapevine DNA methylation and polyphenols content induced by solar ultraviolet-B radiation, water deficit and abscisic acid spray treatments. Plant Physiol. Biochem 135, 287–294 (2019). [PubMed: 30599305]
51. Nandakumar V, Vaid M, Tollefsbol TO & Katiyar SK Aberrant DNA hypermethylation patterns lead to transcriptional silencing of tumor suppressor genes in UVB-exposed skin and UVB-induced skin tumors of mice. Carcinogenesis 32, 597–604 (2011). [PubMed: 21186298]
52. Zhu X et al. Effects of ultraviolet B exposure on DNA methylation in patients with systemic lupus erythematosus. Exp. Ther. Med 5, 1219–1225 (2013). [PubMed: 23596493]
53. Pavet V, Quintero C, Cecchini NM, Rosa AL & Alvarez ME Arabidopsis displays centromeric DNA hypomethylation and cytological alterations of heterochromatin upon attack by Pseudomonas syringae. Mol. Plant-Microbe Interact 19, 577–587 (2006). [PubMed: 16776291]
54. Secco D et al. Stress induced gene expression drives transient DNA methylation changes at adjacent repetitive elements. Elife 4, e09343 (2015).
55. Citterio S et al. Specific hypomethylation of DNA is induced by heavy metals in white clover and industrial hemp. Physiol. Plant 121, 472–480 (2004).
56. Greco M, Chiappetta A, Bruno L & Bitonti MB In Posidonia oceanica cadmium induces changes in DNA methylation and chromatin patterning. J. Exp. Bot 63, 695–709 (2012). [PubMed: 22058406]
57. Gao Z et al. An RNA polymerase II-and AGO4-associated protein acts in RNA-directed DNA methylation. Nature 465, 106–109 (2010). [PubMed: 20410883]
58. Azevedo J et al. UAP56 associates with DRM2 and is localized to chromatin in Arabidopsis. FEBS Open Bio 9, 973–985 (2019).
59. Sasaki T, Lorković ZJ, Liang SC, Matzke AJM & Matzke M The ability to form homodimers is essential for RDM1 to function in RNA-directed DNA methylation. PLoS One 9, 1–8 (2014).
60. Dangwal M, Malik G, Kapoor S & Kapoor M De Novo Methyltransferase, OsDRM2, Interacts with the ATP-Dependent RNA Helicase, OseIF4A, in Rice. J. Mol. Biol 425, 2853–2866 (2013). [PubMed: 23732981]
61. Zhou S et al. Cooperation between the H3K27me3 chromatin mark and non-CG methylation in epigenetic regulation. Plant Physiol. 172, 1131–1141 (2016). [PubMed: 27535791]
62. Rajavelu A et al. Chromatin-dependent allosteric regulation of DNMT3A activity by MeCP2. Nucleic Acids Res. 46, 9044–9056 (2018). [PubMed: 30102379]

63. Zientara-Rytter K & Sirko A Significant role of PB1 and UBA domains in multimerization of Joka2, a selective autophagy cargo receptor from tobacco. Front. Plant Sci 5, 13 (2014). [PubMed: 24550923]
64. Raasi S, Varadan R, Fushman D & Pickart CM Diverse polyubiquitin interaction properties of ubiquitin-associated domains. 12, 708–714 (2005).
65. Sadowski M, Suryadinata R, Tan AR, Roesley SNA & Sarcevic B Protein monoubiquitination and polyubiquitination generate structural diversity to control distinct biological processes. IUBMB Life 64, 136–142 (2012). [PubMed: 22131221]
66. Walbot V UV-B damage amplified by transposons in maize. Nature 397, 398–399 (1999).
67. Zhang T et al. Genome of Crucihimalaya himalaica, a close relative of Arabidopsis, shows ecological adaptation to high altitude. Proc. Natl. Acad. Sci 116, 7137–7146 (2019). [PubMed: 30894495]
68. Quadrana L & Colot V Plant Transgenerational Epigenetics. Annu. Rev. Genet 50, 467–491 (2016). [PubMed: 27732791]
69. Niu X et al. Transposable elements drive rapid phenotypic variation in Capsella rubella. Proc Natl Acad Sci USA 116, 6908–6913 (2019). [PubMed: 30877258]
70. Moissiard G et al. MORC family ATPases required for heterochromatin condensation and gene silencing. Science 336, 1448–1451 (2012). [PubMed: 22555433]
71. Eun C et al. AGO6 Functions in RNA-Mediated Transcriptional Gene Silencing in Shoot and Root Meristems in Arabidopsis thaliana. PLoS One 6, e25730 (2011). [PubMed: 21998686]
72. Xi Y & Li W BSMAP: whole genome bisulfite sequence MAPping program. BMC Bioinformatics 10, 232 (2009). [PubMed: 19635165]
73. Bolger AM, Lohse M & Usadel B Trimmomatic: a flexible trimmer for Illumina sequence data. Bioinformatics 30, 2114–2120 (2014). [PubMed: 24695404]
74. Quinlan AR & Hall IM BEDTools: a flexible suite of utilities for comparing genomic features. Bioinformatics 26, 841–842 (2010). [PubMed: 20110278]
75. Akalin A et al. methylKit: a comprehensive R package for the analysis of genome-wide DNA methylation profiles. Genome Biol. 13, R87 (2012). [PubMed: 23034086]
76. Kim D, Langmead B & Salzberg SL HISAT: a fast spliced aligner with low memory requirements. Nat. Methods 12, 357–360 (2015). [PubMed: 25751142]
77. Trapnell C et al. Transcript assembly and quantification by RNA-Seq reveals unannotated transcripts and isoform switching during cell differentiation. Nat. Biotechnol 28, 511 (2010). [PubMed: 20436464]
78. Stroud H, Greenberg MVC, Feng S, Bernatavichute YV & Jacobsen SE Comprehensive analysis of silencing mutants reveals complex regulation of the Arabidopsis methylome. Cell 152, 352–364 (2013). [PubMed: 23313553]
79. Law JA et al. Polymerase IV occupancy at RNA-directed DNA methylation sites requires SHH1. Nature 498, 385 (2013). [PubMed: 23636332]
80. Tavridou E, Pireyre M & Ulm R Degradation of the transcription factors PIF4 and PIF5 under UV-B promotes UVR8-mediated inhibition of hypocotyl growth in Arabidopsis. Plant J. 101, 507–517 (2020). [PubMed: 31571300]
81. Zhong X et al. Domains rearranged methyltransferase3 controls DNA methylation and regulates RNA polymerase V transcript abundance in Arabidopsis. Proc. Natl. Acad. Sci. U. S. A 112, 911–916 (2015). [PubMed: 25561521]
82. Du J et al. Dual binding of chromomethylase domains to H3K9me2-containing nucleosomes directs DNA methylation in plants. Cell 151, 167–180 (2012). [PubMed: 23021223]
83. Law JA et al. A Protein Complex Required for Polymerase V Transcripts and RNA- Directed DNA Methylation in Arabidopsis. Curr. Biol 20, 951–956 (2010). [PubMed: 20409711]
84. Ausin I et al. INVOLVED IN DE NOVO 2-containing complex involved in RNA-directed DNA methylation in Arabidopsis. Proc. Natl. Acad. Sci. U. S. A 109, 8374–8381 (2012). [PubMed: 22592791]
85. Chen X et al. POWERDRESS interacts with HISTONE DEACETYLASE 9 to promote aging in Arabidopsis. Elife 5, e17214 (2016). [PubMed: 27873573]

86. Mayer KS et al. HDA9-PWR-HOS15 is a core histone deacetylase complex regulating transcription and development. Plant Physiol. 180, 342–355 (2019). [PubMed: 30765479]

87. Chen X et al. Canonical and Noncanonical Actions of Arabidopsis Histone Deacetylases in Ribosomal RNA Processing. Plant Cell 30, 134–152 (2018). [PubMed: 29343504]

88. Yang Z et al. EBS is a bivalent histone reader that regulates floral phase transition in Arabidopsis. Nat. Genet 50, 1247–1253 (2018). [PubMed: 30082787]

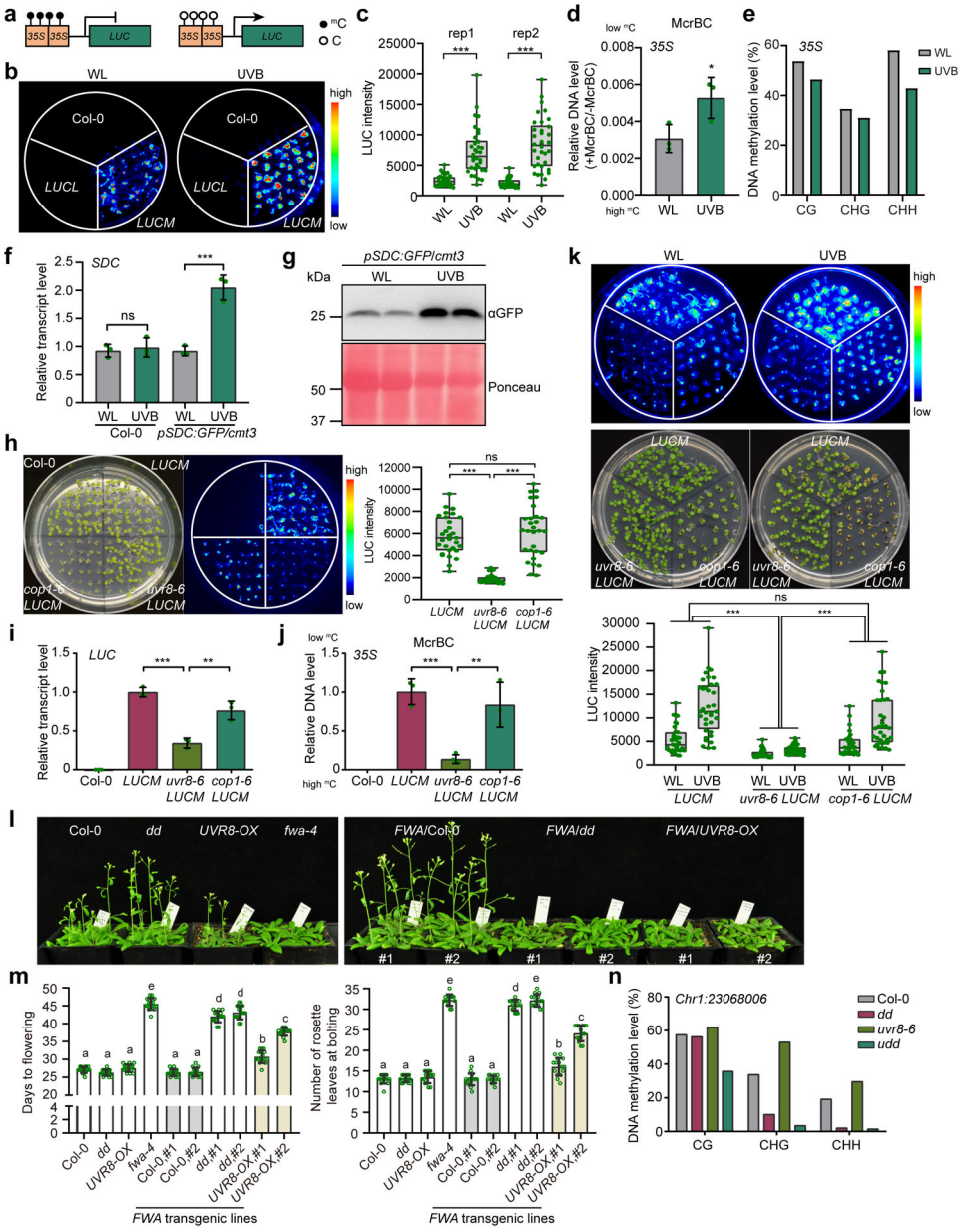

Fig. 1: UVB induces DNA hypomethylation in a UVR8-dependent manner

a, Schematic diagram showing the *d35S:LUC* reporter lines. ^{m}C and C represent methylated and unmethylated cytosine, respectively. **b**, Luciferase images of Col-0 and two *d35S:LUC* reporter lines treated with UVB (~1.5 μE narrowband) for 6 days. *LUCL* and *LUCM* are low and medium LUC expressing lines, respectively. WL, white light. **c**, Quantification of luciferase intensity in (**b**) from two independent biological replicates. Each dot represents a single plant in each group of experiment. The lower and upper box edges correspond to the first and third quartiles, the horizontal lines indicate the median, and the lower and upper whiskers denote the minimal and maximal value, respectively. **d**, McrBC-qPCR based DNA methylation assay of *35S* promoter regions. Low amplification represents high DNA methylation level. Data is mean ± SD. *, p<0.05 by Student's t-test. **e**, Bisulfite sequencing

of *35S* in *LUCM* with white light (WL) or UVB treatment (~1.5 μE narrowband) for 6 days. **f,** Relative RNA transcript level of *SDC* gene in Col-0 and *pSDC:GFP/cmt3* plants grown under white light (WL) and UVB (~1.5 μE narrowband) for 6 days. Data is mean ± SD. ns, not significant; ***, p<0.001 by Student's t-test. **g**, Immunoblot of GFP in *pSDC:GFP/cmt3* in response to UVB. Ponceau staining serves as a loading control.
h, Luciferase images and quantification of intensity of *LUCM* in *uvr8–6* and *cop1–6*. Each dot represents a single plant. The lower and upper box edges correspond to the first and third quartiles, the horizontal line indicates the median, and the lower and upper whiskers denote the minimal and maximal value, respectively. ns, not significant; ***, p<0.001 by Student's t-test. **i**, Relative RNA transcript level of *LUC* in samples in (**h**). Data is mean ± SD. ***, p<0.001; **, p<0.01 by Student's t-test. **j**, McrBC-qPCR based DNA methylation assay of *35S* promoter regions. Low amplification represents high DNA methylation level. Data is mean ± SD. ***, p<0.001; **, p<0.01 by Student's t-test. **k**, Luciferase images and quantification of luciferase intensity of *LUCM* treated with UVB (~1.5 μE) or white light (WL). The lower and upper box edges correspond to the first and third quartiles; the horizontal lines indicate the median, and the lower and upper whiskers correspond to the minimal and maximal value, respectively. ***, p<0.001 by two-way ANOVA test. **l**, Phenotypic images of homozygous *FWA* T_3 transgenic lines in indicated background. The non-transformed plants serve as controls. *dd*, *drm1 drm2*; *fwa-4*, an epiallele mutant of *FWA*; *UVR8-OX*, a homozygous *35S:UVR8-FLAG* overexpressing line. **m,** Quantification of flowering time of *FWA* transgenic plants determined by days to flowering (left panel) and number of rosette leaves at bolting (right panel). Each dot represents a single plant. Data is mean ± SEM. Different letters represent significant differences (p<0.05 by Student's t-test) between samples. **n**, Bisulfite sequencing of *Chr1:23068006* locus (Chr1:23068006–23068366). *dd*, *drm1 drm2*; *udd*, *uvr8–6 drm1 drm2*.

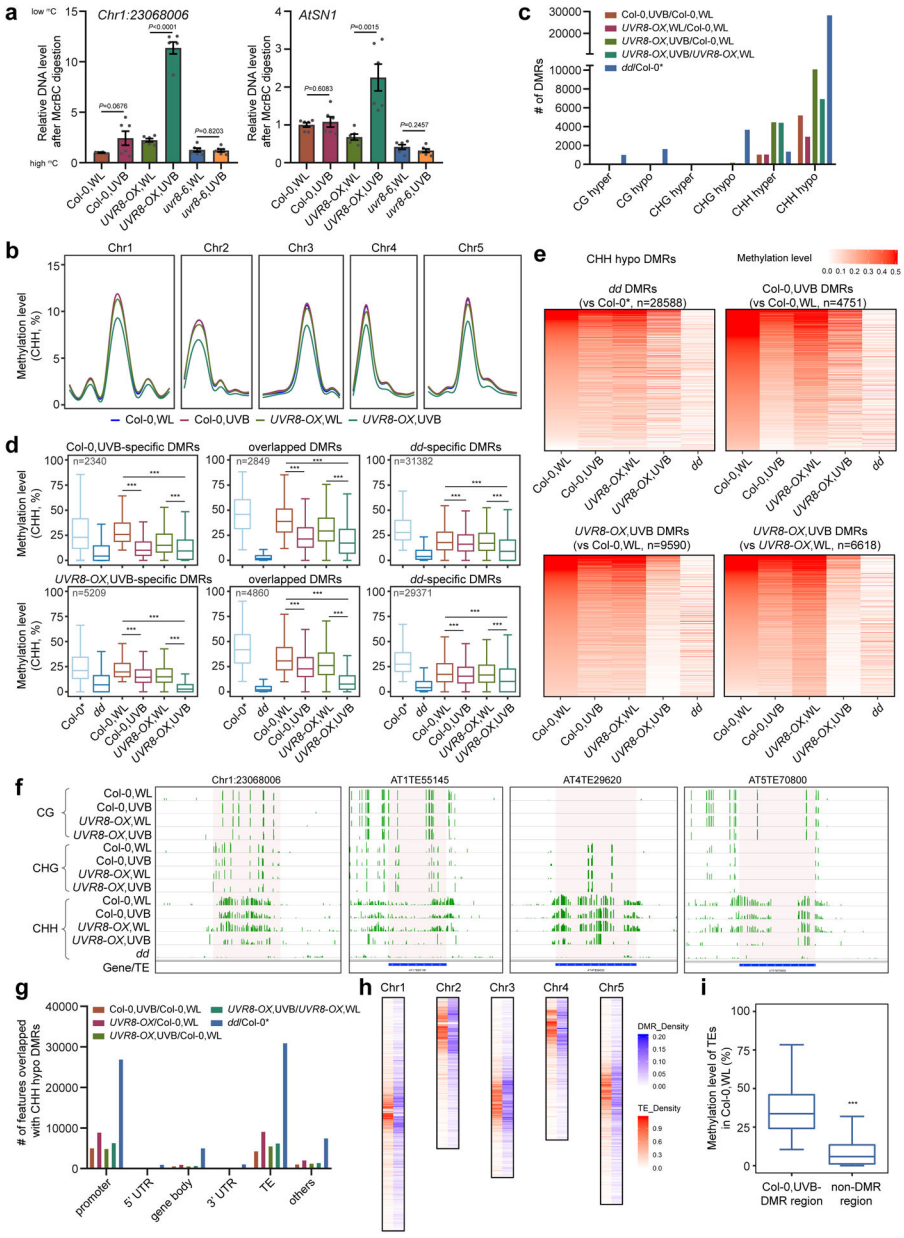

Fig. 2: UVB induces genome-wide CHH hypomethylation

a, McrBC-qPCR based DNA methylation assay of *Chr1:23068006* and *AtSN1* in Col-0, *UVR8-OX*, and *uvr8–6* plants with white light (WL) or UVB treatment (1.5 μE for 10 days). Data is mean ± SEM from two biological replicates with three technical replicates. The *P* values by Student's t-test were shown. **b**, Metaplots showing average CHH methylation levels in Col-0 and *UVR8-OX* plants with or without UVB treatment. Chr1 to Chr5 represent five chromosomes.

c, Numbers of differential methylation regions (DMRs) in context of CG, CHG, and CHH. Col-0* is the control for *drm1 drm2* (*dd*) from ref[78]. **d**, Boxplots of CHH methylation levels of UVB-specific, overlapping, and *dd*-specific DMRs in different samples. The number of DMRs were indicated as 'n'. The DMRs are the overlapping between Col-0,UVB-DMRs

(upper panel) or *UVR8-OX*,UVB-DMRs (lower panel) against Col-0 *dd*-DMRs. The lower and upper box edges correspond to the first and third quartiles, the horizontal lines indicate the median, and the lower and upper whiskers denote the smallest and largest value at most 1.5× IQR, respectively. ***, $p < 0.001$, by nonparametric Mann-Whitney-Wilcoxon test. **e**, Heat-maps showing the CHH methylation levels of different samples in the regions corresponding to the indicated DMRs. **f**, Representative snapshots of UVB-induced CHH hypomethylation regions. The data range is [0,1]. **g**, The distribution of CHH hypo DMRs in the genome. **h**, The density of Col-0,UVB-CHH hypo DMRs and TEs on chromosomes. The density is the proportion of DMRs or TEs in a 100kb window. **i**, CHH methylation levels of TE with or without UVB-induced CHH hypo DMRs. The lower and upper box edges correspond to the first and third quartiles, the horizontal lines indicate the median, and the lower and upper whiskers denote the smallest and largest value at most 1.5× IQR, respectively. ***, $p < 0.001$, by nonparametric Mann-Whitney-Wilcoxon test.

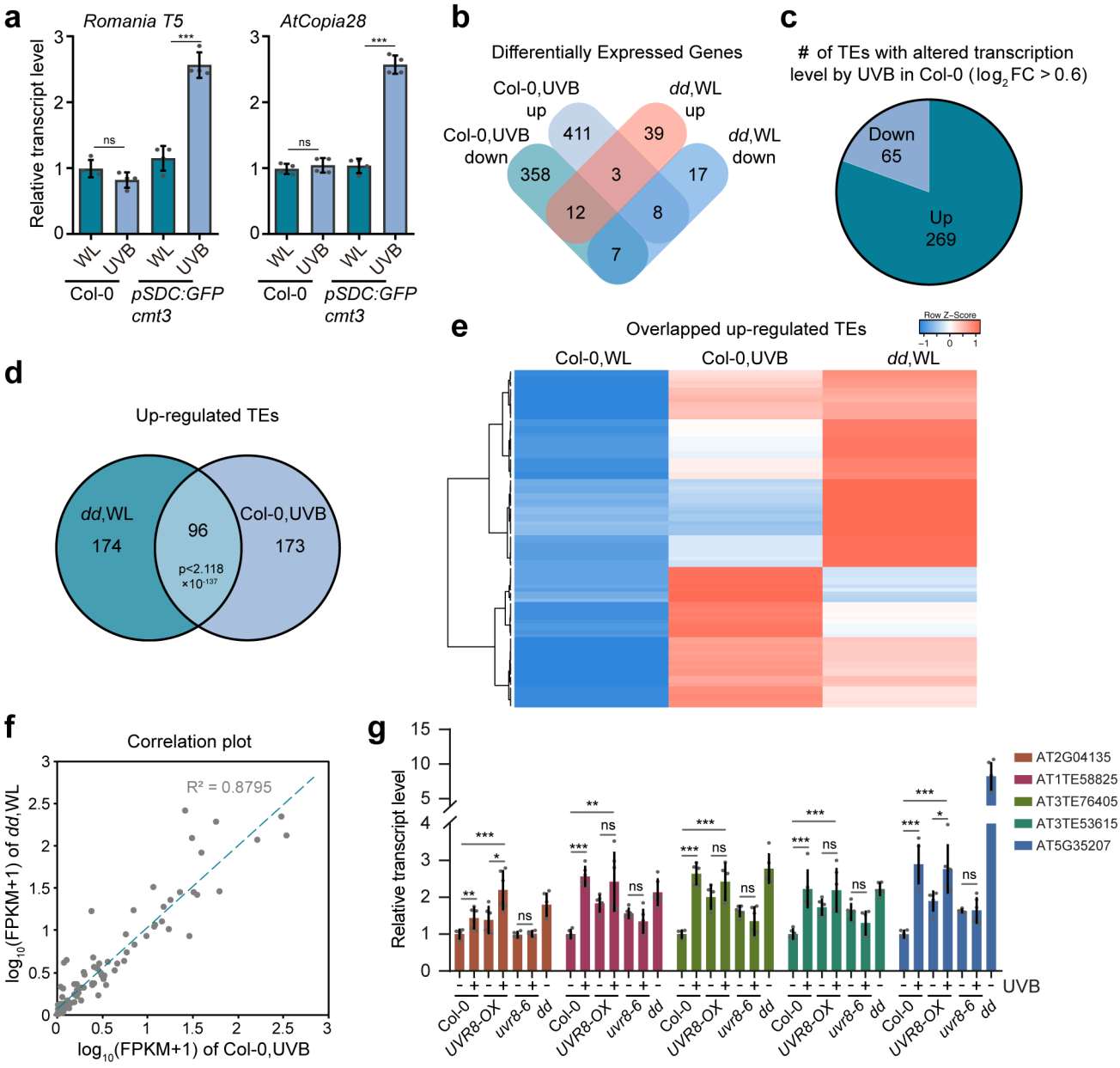

Fig. 3: UVB and DRM2 regulate expression of TEs

a, Relative RNA transcript levels of *Romania T5* and *AtCopia28*. Data is mean ± SD. ns, not significant; ***, $p < 0.001$ by Student's *t*-test. **b**, Venn diagram showing the overlap of differentially expressed genes (DEGs, $q < 0.05$) in UVB treated Col-0 with those of *drm1 drm2* (*dd*). The DEGs were defined against Col-0 without UVB treatment. WL, white light. **c**, Number of UVB up-regulated and down-regulated TEs based on fold-change ($log_2FC > 0.6$) in RNA-seq. **d**, Venn diagram showing the significant overlap of up-regulated TEs in Col-0 treated with UVB and *dd* mutant. **e**, Heat-map showing the expression levels of common up-regulated TE in *dd* and UVB-treated Col-0. **f**, Correlation plot of the expression of the common up-regulated TEs in *dd* and UVB-treated Col-0 (n = 96). **g**, RT-qPCR showing the expression of TEs in Col-0, *UVR8-OX*, and *uvr8–6* with or without UVB

treatment, and *dd*. Data are mean ± SD from two biological replicates with three technical replicates each. *, $p < 0.05$; **, $p<0.01$; ***, $p<0.001$; ns, not significant by Student's *t*-test.

a

Protein	Replicate 1 Spectra	UniqPepts	% Coverage	NSAFe5	Replicate 2 Spectra	UniqPepts	% Coverage	NSAFe5
DRM2	310	37	43.30	1025.469	331	32	45.80	2500.501
AGO4 *	35	20	22.10	78.439	15	8	10.40	76.77
UVR8	9	6	16.40	42.357	8	7	21.60	85.983
MSI4 *	25	8	21.30	102.11	3	2	5.90	27.98
HTB9 *	10	5	35.30	138.052	12	5	35.30	378.323
TPR2	11	7	5.40	20.14	5	5	4.60	20.906

* Listed in Zhong et al. (2014)

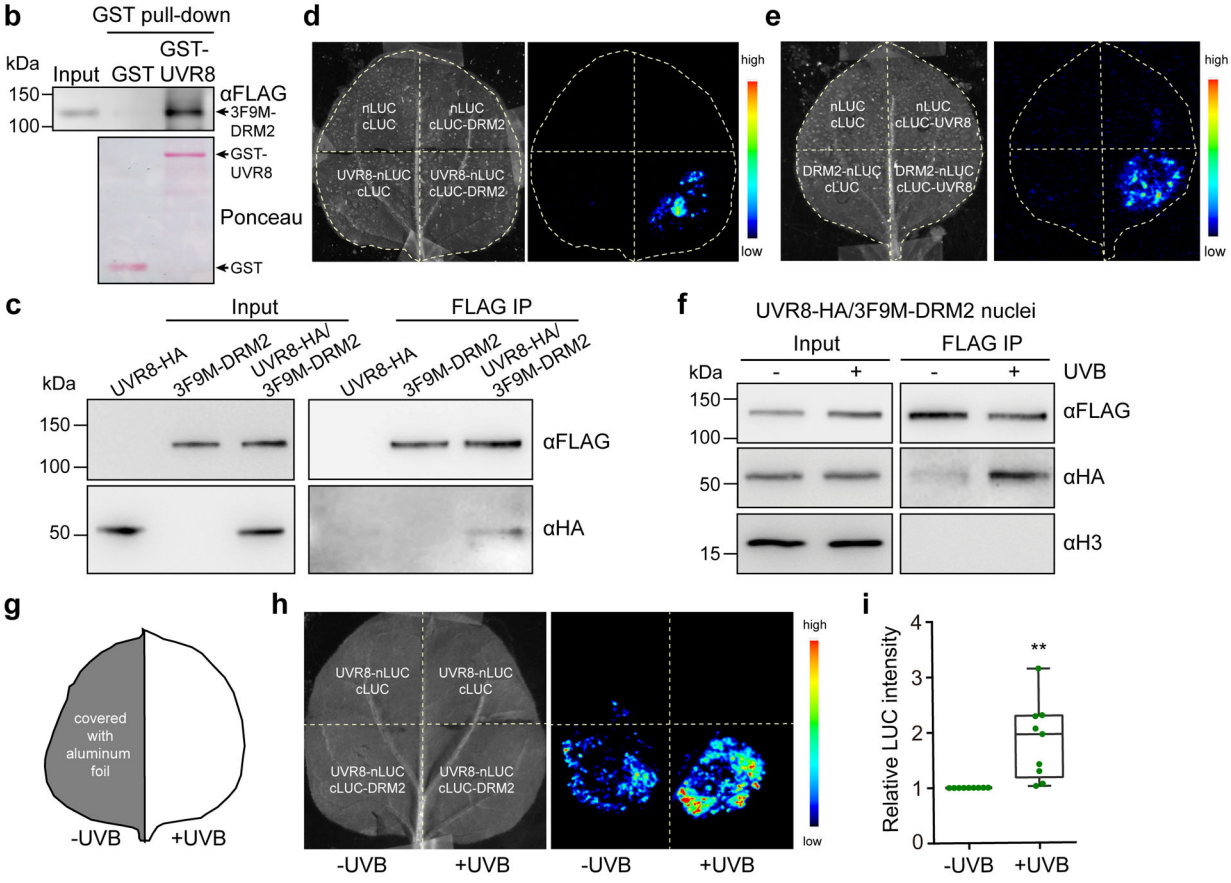

Fig. 4: DRM2 interacts with UVR8 *in vitro* and *in vivo*

a, List of partial proteins co-purified with DRM2 (original data in ref[34]). "UniqPepts" indicates the number of unique peptides that are mapped to one single protein; "%Coverage" indicates the percentage of the protein covered by unique peptides; NSAFe5 indicates normalized spectral abundance factor. Full list is included in Supplementary Dataset 1. **b**, GST pull-down assay using GST-UVR8 purified from *E. coli* and DRM2 purified from *3F9M-DRM2* transgenic plants.

c, Co-immunoprecipitation of UVR8 and DRM2 with FLAG beads using nuclei isolated from 10-d old Arabidopsis seedlings expressing UVR8-HA and/or DRM2-FLAG. **d** and **e**, Split luciferase assay in *N. benthamiana* leaves co-expressing the indicated constructs. UVR8-nLuc and cLuc-DRM2 (**d**) or cLuc-UVR8 and DRM2-nLuc (**e**) were co-expressed in *N. benthamiana* leaves and imaged after spraying with luciferin. nLuc- and cLuc-only

vectors serve as negative controls. **f,** Co-immunoprecipitation of UVR8 and DRM2 using nuclei isolated from 10-d-old *UVR8-HA/3F9M-DRM2* Arabidopsis seedlings treated with or without ~1.5 μE UVB for 4 hours. Histone H3 serves as a nuclear marker. **g**, Diagram showing the UVB treatment in split luciferase assay. '+UVB' indicates the half leaf with 30 minutes of UVB treatment under broadband UVB fluorescent lamp. ' -UVB' indicates the half leaf covered with aluminum foil. **h**, Split luciferase assay showing that UVB enhances UVR8-DRM2 interaction. **i**, Quantification of the luciferase signal in (**h**). The LUC signals are normalized to -UVB control in each biological replicate. Each dot represents a single biological replicate. Data from nine biological replicates were shown. The lower and upper box edges correspond to the first and third quartiles, the horizontal line indicates the median, and the lower and upper whiskers correspond to the minimal and maximal value, respectively. **, $p<0.01$ by student's *t*-test.

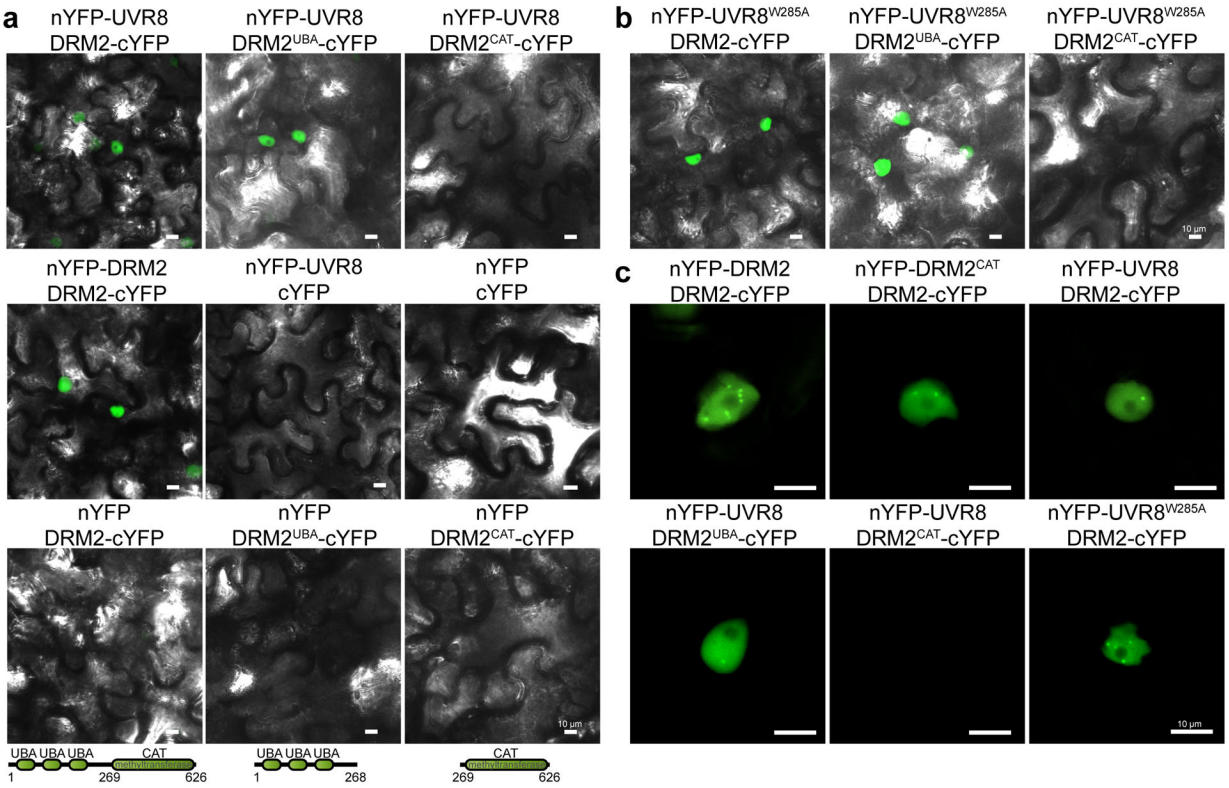

Fig. 5: UBA domains of DRM2 mediate its interaction with UVR8

a, Bimolecular fluorescence complementation assay (BIFC) in *N. benthamiana* leaves co-expressing the indicated constructs. $DRM2^{UBA}$ is a partial DRM2 protein containing only UBA domains (1–268 aa). $DRM2^{CAT}$ is a partial DRM2 protein containing only methyltransferase domain (269–626 aa). nYFP and cYFP represent the N- and C-terminus of YFP protein, respectively. Scale bar, 10 μm. **b**, BIFC assay in *N. benthamiana* leaves showing the interaction between constitutively monomeric $UVR8^{W285A}$ and DRM2, $DRM2^{UBA}$, and $DRM2^{CAT}$. Scale bar, 10 μm. **c**, Magnified images showing the DRM2 homodimerization and UVR8-DRM2 interaction in the nuclear bodies. Scale bar, 10 μm.

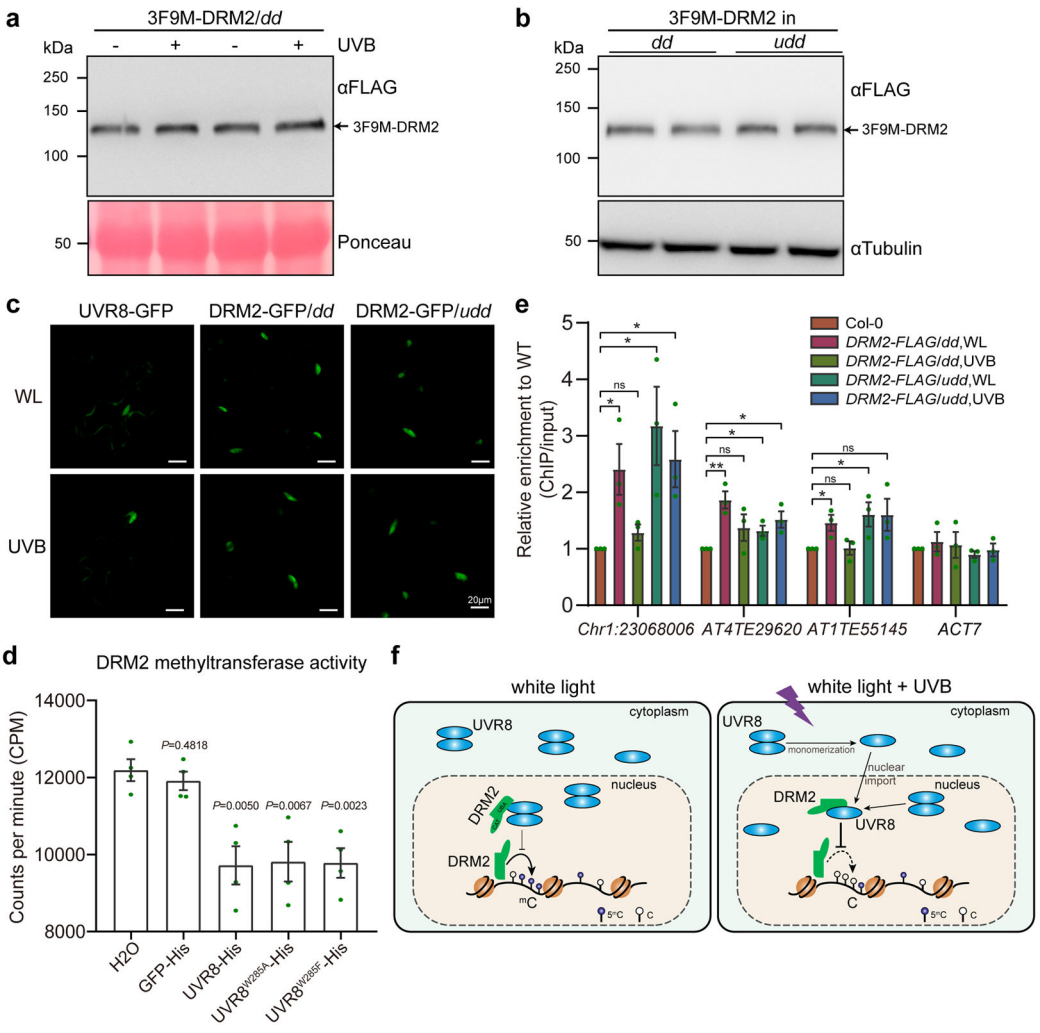

Fig. 6: UVR8 inhibits the methyltransferase activity and chromatin association of DRM2

a and **b**, Western blot showing the DRM2 protein abundance upon UVB treatment (**a**) and in *uvr8–6 drm1 drm2* (*udd*) mutant (**b**). **c**, Subcellular localization of UVR8-GFP, DRM2-GFP in *dd* and *udd* with and without UVB treatment (~1.5 μmol·m^{-2}·s^{-1} narrowband UVB for 4 h) in *Arabidopsis*. WL, white light. Scale bar, 20 μm. **d**, *In vitro* DRM2 methyltransferase activity assay. The concentration of DRM2 (59–626) and His-tagged proteins is 0.2 μM and 3.0 μM, respectively. GFP-His and H_2O serve as controls. Data is mean ± SEM from 4 biological replicates. The *P* value by Student's t-test against H_2O control were shown. **e**, ChIP-qPCR showing DRM2 enrichment at selected loci with and without UVB treatment using *DRM2-FLAG*/*dd* and *DRM2-FLAG*/*udd* transgenic plants. *ACT7* serves as a control. Data are mean ± SEM from 3 biological replicates. ns, not significant. *, p<0.05; **, p<0.01 by Student's *t*-test. **f**, A working model of UVR8-mediated UVB perception and DNA methylation suppression. Under white light, UVR8 predominantly localizes in the cytosol as a homodimer with a small portion in the nucleus. The nuclear UVR8 interacts with and weakly inhibits DRM2 activity at a basal level. Upon UVB irradiation, UVR8 perceives UVB and undergoes monomerization followed by nuclear import. In the nucleus, UVR8

interacts with DRM2 and induces DNA hypomethylation by inhibiting the methyltransferase activity and chromatin association of DRM2.